Reviews in Mineralogy & Geochemistry
Vol. 89 pp. 339-372, 2023

Lunar Impact Features and Processes

Gordon R. Osinski[1,2,3], H. Jay Melosh[4*], Jeff Andrews-Hanna[5], David Baker[6], Brett Denevi[7], Deepak Dhingra[8], Rebecca Ghent[9], Paul O. Hayne[10], Patrick Hill[1,2,3], Peter B. James[11], Steven Jaret[12], Brandon Johnson[13], Thomas Kenkmann[14], David Kring[15], Prasun Mahanti[16], David Minton[4], Catherine D. Neish[1,2,3], Greg Neumann[6], Jeff Plescia[7], Ross W. K. Potter[13], Jim Richardson[9], Elizabeth A. Silber[1,2,3], Jason M. Soderblom[17], Michael Zanetti[1,2,3,18], Nicolle Zellner[19]

[1]Department of Earth Sciences, University of Western Ontario, 1151 Richmond St. London, ON, N6A 5B7, Canada
[2]Institute for Earth and Space Exploration, University of Western Ontario, 1151 Richmond St., London, ON, N6A 5B7, Canada
[3]Canadian Lunar Research Network, University of Western Ontario, 1151 Richmond St. London, ON, N6A 5B7, Canada
[4]Earth Atmospheric and Planetary Sciences, Purdue University West Lafayette IN 47907, USA
[5]Lunar and Planetary Lab, University of Arizona, Tucson, AZ 85721, USA
[6]Planetary Geology, Geophysics and Geochemistry Lab, Code 698, Goddard Space Flight Center, Greenbelt, MD 20771, USA
[7]Applied Physics Laboratory, Johns Hopkins University, Laurel, MD 20723, USA
[8]Department of Earth Sciences, Indian Institute of Technology Kanpur Kalyanpur, Kanpur 208016, Uttar Pradesh, India
[9]Planetary Science Institute, 1700 E. Fort Lowell, Tucson, AZ 85719, USA
[10]Department of Astrophysical and Planetary Sciences University of Colorado Boulder, CO 80309, USA
[11]Department of Geosciences, Baylor University, Waco, TX 76798, USA
[12]American Museum of Natural History, New York, New York, 10024, USA
[13]Department of Earth, Environmental and Planetary Sciences Brown University, Providence, RI 02912, USA
[14]Institut fur Geo- und Umweltnaturwissenschaften, Albert-Ludwigs-Universität Freiburg, Freiberg, Germany
[15]Center for Lunar and Space Exploration, Lunar and Planetary Institute 3600 Bay Area Blvd., Houston, TX 77058, USA
[16]School of Earth and Space Exploration, Arizona State University Tempe, AZ 85281, USA
[17]Earth, Atmospheric and Planetary Sciences, Massachusetts Institute of Technology, Cambridge, MA 02139, USA
[18]NASA George C. Marshall Space Flight Center National Space Science and Technology Center, 320 Sparkman Drive Huntsville, AL 35805, USA
[19]Department of Physics, Albion College, Albion MI 49224, USA
**Deceased*

gosinski@uwo.ca

1529-6466/23/0089-0008$05.00 (print)
1943-2666/23/0089-0008$05.00 (online)
http://dx.doi.org/10.2138/rmg.2023.89.08

DEDICATION

This chapter is dedicated to H. Jay Melosh who tragically passed away during this endeavor. From his earliest publications on the concept of acoustic fluidization, to the publication of his landmark book *Impact Cratering—A Geologic Process* in 1989, to his latest contributions to the paper by Trowbridge et al. (2020) cited herein on understanding of the South Pole-Aiken basin, Jay's contributions to the understanding of the impact cratering process, and planetary surface processes in general, are unparalleled. His passing leaves a huge void in the community and he will be sorely missed.

1. PREFACE

Impact craters are the Moon's quintessential landform. First recognized by Galileo in 1610, craters dominate the lunar landscape and, as we know from the subsurface probing Gravity Recovery and Interior Laboratory (GRAIL) mission, impact events have affected the lunar crust down to depths of at least tens of kilometers. Since the publication of the first New Views of the Moon book, new missions such as Kaguya (SELENE), Chandrayaan-1, Lunar Reconnaissance Orbiter (LRO), Chang'E (1–4), and GRAIL, among others, have provided large amounts of new data. Laboratory investigations of both Apollo and lunar meteorite samples have continued to improve our understanding of the role of impacts in the origin and evolution of the Moon (see also Cohen et al. 2023, this volume), and computer codes for the simulation of crater formation and landscape evolution have improved greatly. Taken together, our understanding of the impact cratering process and its role in shaping not just the surface and interior of the Moon, but of rocky and icy planetary objects in general, has improved dramatically in the past decade. This chapter is a necessarily abbreviated summary of the progress in the field since the publication of New Views of the Moon (NVM-1) in 2006.

2. THE BASICS OF IMPACT CRATERING

Impact cratering is a complex and dynamic process. The formation of hypervelocity impact craters is conventionally divided into three main stages (Gault et al. 1968) (Fig. 1) (1) contact and compression, (2) excavation, and (3) modification or collapse. Below we provide a concise overview of the impact cratering process. It is beyond the scope of this chapter to provide a detailed overview of the processes, products and effects of impact events; comprehensive treatises of the many facets of impact cratering are provided by Roddy et al. (1977), Melosh (1989), French (1998), and Osinski and Pierazzo (2012).

2.1. Contact and compression

The first stage of an impact event begins when the projectile strikes the surface; the impactor immediately decelerates as it compresses and subsequently pushes target material out of its path (Melosh 2012). The rapid compression of the impactor and target creates shock waves that initiate at the contact point and then propagate away—faster than the speed of sound—into both entities (Fig. 1). After this brief compression (seconds for km scale projectiles), rarefaction or release waves are initiated at target and impactor surfaces and propagate into the interior of the projectile (Ahrens and O'Keefe 1972). The passage of this rarefaction wave through the projectile allows both the pressure and temperature to drop along a near-adiabatic path back to low pressure; upon release, temperatures remain high enough that the projectile is invariably completely melted and/or vaporized (Gault et al. 1968; Melosh 1989). The increase in internal energy accompanying shock compression and subsequent rarefaction also results in the fracturing, shock metamorphism (see separate section below), melting (see separate section below), and/or vaporization of a volume of target material close to the point of impact.

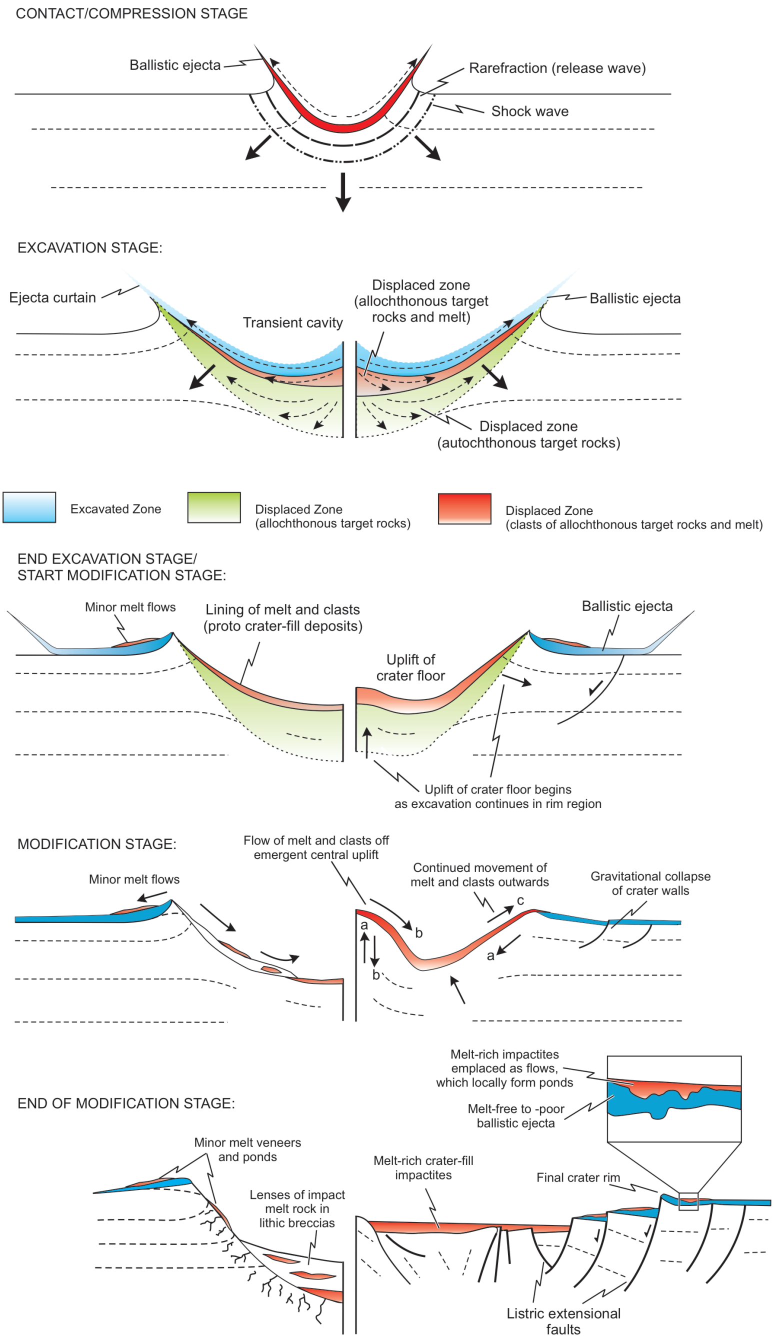

Figure 1. Series of schematic cross sections depicting the 3 main stages in the formation of impact craters. This multi-stage model accounts for melt emplacement in both simple (**left half**) and complex craters (**right half**). For the modification stage section, the arrows represent different time steps, labelled "a" to "c". Initially, the gravitational collapse of crater walls and central uplift **(a)** results in predominantly inward movement of material. Later, melt and clasts flow off the central uplift **(b)**. There is then continued movement of melt and clasts outwards once crater wall collapse has largely ceased **(c)**. Modified from Osinski et al. (2011).

The end of the contact and compression stage is generally taken to be the point when the rarefaction wave has completely released the impactor from high pressure, although the transition to the excavation stage is continuous.

2.2. Excavation

During the excavation stage, the approximately hemispherical shock wave continues to propagate out into the target sequence (Osinski et al. 2012), gradually attenuating and eventually degrading into a normal stress wave (Melosh 1989) (Fig. 1). The expanding shock wave and following rarefaction sets the target material into motion (Melosh 1985). Additional interactions between the shock wave and the surface produces an excavation flow-field that opens a *transient cavity* (e.g., Grieve and Cintala 1981). As the transient cavity grows, the different trajectories of material in different regions of the excavation flow field partition the target into an upper *excavated zone* and a lower *displaced zone*. It is widely accepted that material in the upper excavated zone is ejected ballistically beyond the (still evolving) transient cavity rim to form the continuous ejecta blanket (Oberbeck 1975). At the end of the excavation stage, the transient cavity is lined by a mixture of melt and clasts overlying fractured bedrock (Fig. 1).

Unlike crater shape, which remains approximately circular down to very shallow impact angles, the ejecta curtain and deposition of ejecta are sensitive to impact angle. At angles less than 45° to the horizontal, ejecta is not deposited in the up-range direction, forming a so-called forbidden zone. At very low angles of <20°, the development of a second forbidden zone down-range of the crater occurs, leading to the characteristic butterfly pattern of ejecta deposits (Gault and Wedekind 1978). The maximum depth from which material is ejected is predicted to be ~1/3 of the transient crater depth, but ground-truth observations are scarce, largely due to the erosion of most ejecta blankets on the Earth. The best estimates are from the 1.2 km diameter Barringer Crater (>0.08*D*) (Shoemaker 1963) and the 23 km diameter Haughton and 24 km diameter Ries impact structures (0.05*D*) (Osinski et al. 2011), where *D* is the final rim-to-rim diameter. These estimates are substantially shallower than theoretical estimates, which could be due to small sample size, target lithology effects, or incomplete understanding of the cratering process at large scales.

2.3. Modification

In small meter- to km-size craters, the transient cavity is relatively stable and undergoes relatively minor collapse of the steepest part of the crater rim (Fig. 1), enlarging the diameter by 20–30% (Grieve and Garvin 1984), producing simple craters (Fig. 2A) (see separate section below). In larger so-called complex craters (Fig. 2B) (see separate section below); however, the transient cavity is gravitationally unstable and undergoes collapse during the final modification stage of crater formation (Kenkmann et al. 2012). Two competing processes work during this stage. Initially, the inward and upward movement of material within the transient cavity lifts the crater floor, leading to the development of a central uplift (Fig. 1). With increasing crater diameter, the morphology and morphometry of central uplifts evolves into peak rings (Fig. 2C) (see separate section below). Simultaneously, the initially steep walls of the transient cavity collapse inward and downward as a series of large (~100 m to km scale) fault-bounded blocks. The diameter at which the transition occurs from simple to complex craters depends on the strength of the gravitational field of the parent body and increases with decreasing acceleration due to gravity (Pike 1980a; Melosh 1989); this is discussed below with respect to lunar craters. The apparent strength of the target rock during the modification stage is very low (Melosh 1989): only a few bars (kPa) and with little or no internal friction. The physical explanation for this temporary strength degradation is not well understood. Leading theories include acoustic fluidization (Melosh and Ivanov 1999) and dynamic fault weakening (Senft and Stewart 2009).

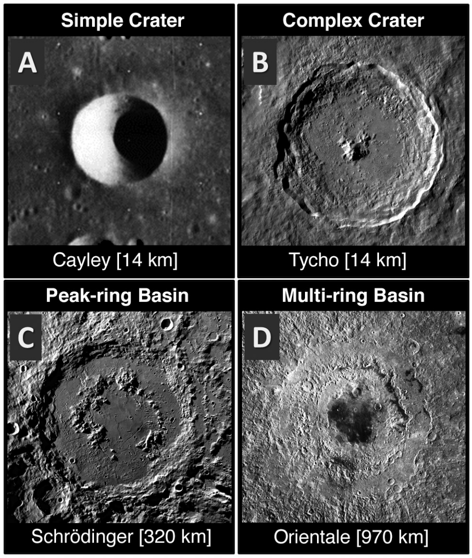

Figure 2. Illustration of the change in morphology of lunar craters with increasing diameter. Images: Portions of LROC WAC mosaics. Image credits: NASA/GSFC/Arizona State University.

2.4. Basic scaling of crater dimensions

The final size of lunar impact craters depends ultimately upon the size, density, velocity, and angle of impact of the projectiles, as well as the density and strength of the target rocks. A well-developed series of scaling relations link these quantities. Although calibrated experiments to verify these relations for km scale craters are not possible with current technologies, recent numerical modeling (Elbeshausen et al. 2009) supports the "Pi-group scaling" approach (Holsapple 1993) and provides power-law relations that are now widely adopted.

3. METHODS OF STUDY

The impact record on Earth remains of fundamental importance for understanding the processes and products of impact cratering not just on the Moon, but throughout the Solar System. In particular, the study of craters on Earth provides the only source of ground-truth data on the three-dimensional structural and lithological character of impact craters (e.g., Grieve and Therriault 2004). The number of confirmed impact craters on Earth now stands at ~200 (Osinski and Grieve 2019) (see www.impactearth.com for an up-to-date listing) and field studies of terrestrial impact structures continue to yield important information about topics such as the formation of complex craters (e.g., Kenkmann et al. 2014; Riller et al. 2018), the generation and emplacement of impactites (e.g., Siegert et al. 2017; Mader and Osinski 2018), and shock metamorphism in lunar-relevant materials (e.g., Pittarello et al. 2020; Xie et al. 2020).

Since the publication of NVM-1 in 2006, a series of orbital and surface missions have increased the volume of lunar data by orders of magnitude, the analysis of which has provided new insight into the impact cratering process. Global coverage of high resolution imagery from instruments such as the Kaguya Terrain Camera (TC) (Haruyama et al. 2008), Lunar Reconnaissance Orbiter Camera (LROC) Wide Angle Camera (WAC), and LROC Narrow Angle Camera (NAC) have enabled new observations of general crater morphology and detailed examination of crater facies (Robinson et al. 2010). Global topography data from the Lunar Orbiter Laser Altimeter (LOLA)

(Smith et al. 2010), and photometrically derived digital elevation models (DEMs) from the Kaguya TC and LROC WAC (Scholten et al. 2012; Barker et al. 2016) complement the imagery and provide morphometric measurements. DEMs from LROC NAC (Henriksen et al. 2017) provide the ability to quantify morphometry at ultra-high resolutions. Compositional datasets from the Kaguya Multiband Imager (MI) (Ohtake et al. 2008) and Gamma Ray Spectrometer (GRS) (Hasebe et al. 2008), the Chandrayaan-1 Moon Mineralogy Mapper (M^3) (Green et al. 2011), the LRO Diviner Radiometer (Paige et al. 2010), and LROC WAC color products (Sato et al. 2014) have expanded our understanding of the global distribution of lithologies exposed and/or modified by the cratering process since the previous generation of orbital spectral data. Orbital synthetic aperture radar (SAR) observations from the LRO Miniature Radio Frequency (Mini-RF) instrument (Nozette et al. 2010), in addition to Diviner radiometer derived thermophysical properties, have provided insight into the physical properties of crater facies. Finally, GRAIL gravity data have revolutionized our understanding of the effects of impacts on the crust by providing data on the subsurface density and porosity structure (Zuber et al. 2013). These global studies are now complemented by local investigations of dielectric properties of the lunar surface from the Chang'E 3 and Chang'E 4 ground-penetrating radar instruments (Lai et al. 2019).

In addition to the study of impact craters on Earth and the Moon, numerical modeling of impacts (see review by Collins et al. 2012) and small-scale laboratory experiments (e.g., Fritz et al. 2019; Johnson et al. 2020) provide important insights into the processes and products of impact cratering. While experimental techniques offer a valuable insight into impact processes at small scales, numerical modeling has proven to be an essential tool for studying impact dynamics at large scales and under a variety of conditions that would not be otherwise replicable in a laboratory. Oftentimes, even at smaller scales, it is challenging to experimentally reproduce the environment (e.g., gravity) that would accurately replicate that of various bodies in the Solar System (Pierazzo et al. 2008).

The development and advancements of shock-physics codes in recent decades have significantly improved our understanding of impact processes on solid planetary bodies, including the Moon. The modern codes, such as iSALE, include a sophisticated description for a wide range of materials (e.g., impactor and target rock composition), including their strength response and behavior under high temperature and pressure (Pierazzo and Melosh 2000a; Collins et al. 2004; Wünnemann et al. 2006, 2008). Numerical models also allow for systematic studies that include testing of a wide parameter space in order to investigate conditions under which a given impact crater might have formed. In turn, constraining such conditions can provide important clues as to history and evolution of the Moon (e.g., Potter et al. 2013; Milbury et al. 2015; Zhu et al. 2015; Johnson et al. 2016). To study the in-situ fracturing and development of the megaregolith, the capability to simulate dynamic fragmentation has also recently been added to iSALE (Wiggins et al. 2019).

Laboratory experiments and observational techniques, on the other hand, provide constraints for numerical models, working in synergy towards the common goal of better understanding impact crater formation at all scales and at all impact process stages (e.g., Poelchau et al. 2014; Morgan et al. 2016).

4. MORPHOLOGY AND MORPHOMETRY OF LUNAR IMPACT CRATERS

For well over a century (Gilbert 1893) it has been recognized that there is a progressive and systematic change in the morphology of craters with increasing size on the Moon (Fig. 2); a relationship that was subsequently shown to hold for all other planetary objects in the Solar System where sufficient data is available. In general, impact craters may be subdivided into three main groups on the basis of morphology: simple, complex, and basins (Fig. 2), with transitional types existing between these three major classes.

4.1. Simple craters

Simple craters are circular depressions with an uplifted rim (Figs. 2A, 3A) (Shoemaker 1960). Long thought to be bowl-shaped and parabolic in shape (Shoemaker 1960), the availability of high-resolution imagery and digital terrain models for the Moon suggests that most simple craters are parabolic in shape (Chappelow 2013). Field studies of terrestrial craters have shown that simple craters are lined with an allochthonous breccia lens composed largely of unshocked target material (Fig. 3A), mixed with discrete cm-size particles and/or m to hundred m-scale lenses of impact melt rock (Shoemaker 1960; Grieve 1978). Veneers and ponds of impact melt are also commonplace, draping crater walls and atop ballistic ejecta blankets of simple craters on the Moon (see separate section below). Studies of terrestrial craters have also revealed that the uplifted rim comprises, in part, a flap of overturned stratigraphy (Shoemaker 1960).

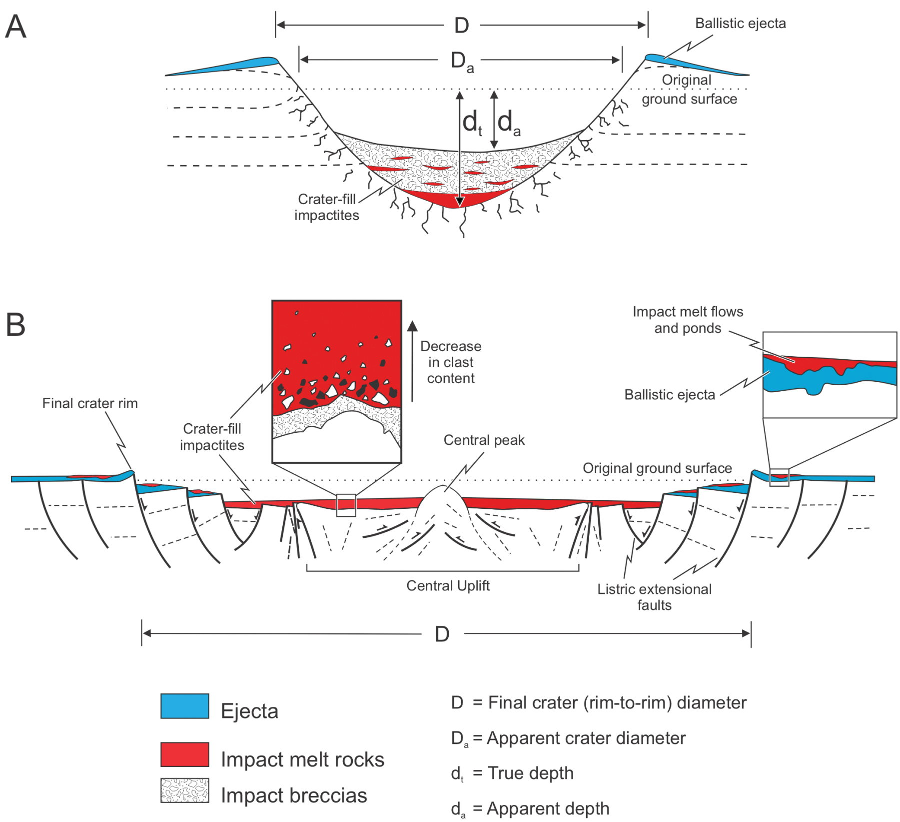

Figure 3. Schematic cross-sections of simple **(A)** and complex **(B)** impact craters. The example shown for (B) is of a central peak crater.

Historically, the typical rim-to-floor depth (*d*) to rim-to-rim diameter (*D*) ratios cited for lunar craters ranged from ~1:5 to 1:7 (Pike 1976) (Fig. 4). More recently, the simple-to-complex transition of lunar craters has more precisely been defined based on a high-resolution, global lunar impact crater database, comprising of 5,505 pristine craters with $D \geq$ ~3 km (Krüger et al. 2018). The best representation for the *d/D* relationship for simple craters is reported as $d = 0.18\ b^{1.05}$, where *b* is the minor axis of the crater outline (Krüger et al. 2018). However, it is notable that the *d/D* ratio for most of the small ($D < 300$ m) fresh simple craters on the surface of the Moon is lower at <0.17 (e.g., Mahanti et al. 2015; Stopar et al. 2017). One hypothesis for this observation is that these smaller craters form on less cohesive and fragmented regolith, and at either the late stages of formation or just after formation, there is a collapse (or a combination of creep and collapse) of the crater walls, reducing the transient *d/D*. Seismic events (either tectonism or impacts) (Schultz and Gault 1975) may trigger such collapse.

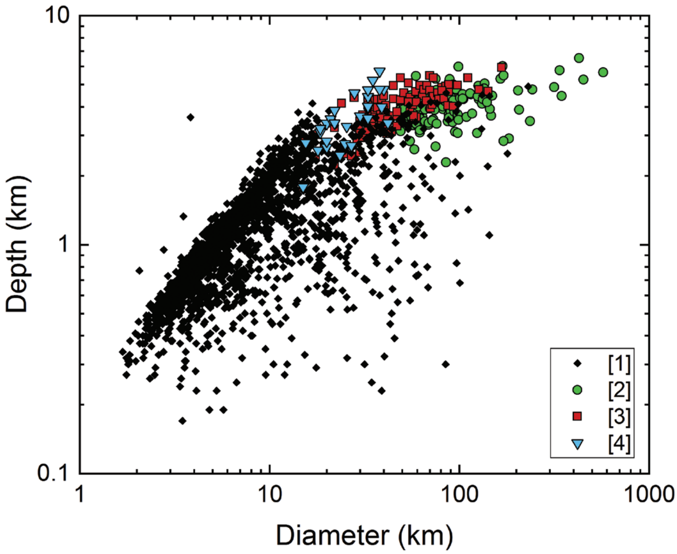

Figure 4. Depth versus diameter for lunar craters. The data sets used are as follows: **Diamonds**: [1] Losiak et al. (2008), updated by T. Ohman (2015), Lunar Impact Database, LPI. **Circles**: Baker and Head (2013) Squares: [3] Kalynn et al. (2013). **Triangles**: [4] Osinski et al. (2018).

In addition to being shallower at formation, smaller craters degrade much more quickly than larger craters. Most of the smaller craters observed on the lunar surface are degraded ($d/D < 0.1$) (Fassett and Thomson 2014), resulting in a landscape dominated by shallow, inverted cone-shaped craters. The rate of degradation of craters progressively declines with change in the morphological state of the crater such that more time is spent in a more degraded state—more than half of the total crater evolution time (from formation to obliteration) is spent as degraded (Mahanti et al. 2018).

Krüger et al. (2018) found that about 73% of the investigated simple craters have circular planforms with aspect ratios ε of less than 1.1; 23.5% show crater aspect ratios between ε = 1.1–1.2, and about 3.5% have an ellipticity larger that ε ≥ 1.2. The ellipticity of crater planforms can be related to impact angles (e.g., Gault and Wedekind 1978). The probability of an impact occurring at an angle θ or less, measured from the surface, is $\sin^2\theta$ (Shoemaker 1963). An impact with 10° has a probability of 3%, which is similar to the number of simple crater with elliptical planforms of ε ≥ 1.2.

The diameter at which simple-to-complex transition occurs is approximately inversely proportional to the gravitational acceleration (g) (Pike 1980a; Melosh 1989) and, therefore, varies systematically among different planetary bodies. The transition from simple to so-called complex impact craters on the Moon was initially proposed to occur at ~19 km (Pike 1977, 1980b), although it was noted that there is a target-dependent variation in the transitional crater diameter, with ~21 km on the highlands and ~16 km on mare typically cited. More recently, Krüger et al. (2018)

derived a robust simple-to-complex crater transition diameter at 20.1 km for highland craters, 17.7 km for mare craters, and 18.8 km for the global crater population. However, it is important to note that the transition from simple to complex craters is not abrupt (Fig. 4) and, furthermore, that a sub-group of craters dubbed "transitional", occur in this size range.

4.2. Transitional craters

A *transitional* crater can be defined as a flat-floored crater that does not display the bowl-shaped form of simple craters, possesses one or more discrete terraces and/or rock slides, but that lacks a centrally uplifted region that is emergent through the allochthonous crater-fill impactites (i.e., a central peak) (Krüger et al. 2018; Osinski et al. 2019). These craters have relatively shallow depths (Fig. 4), may possess faulted "terraced" rims similar to complex craters, and exhibit flat floors that are completely or partly covered with impactites (Fig. 5). In the past, some authors have labeled craters possessing a central peak as *transitional*; however, given the fundamental requirement of the existence of a central peak in the definition of a complex crater (Dence 1964) (and see next section), the above definition is recommended. As with simple craters, the morphology and morphometry of transitional craters is affected by target properties. One such striking contrast exists between the transitional craters Giordano Bruno and Picard. Both are approximately 22 km in diameter, but have notably different morphologies and depths; Giordano Bruno (*d* ~ 3.9 km; Fig. 5D) is situated in the lunar highlands and Picard (d ~ 2.5 km; Fig. 5B) formed in a mare target. It has been proposed that layering in mare targets is the major driver for these differences. Layering provides pre-existing planes of weakness that facilitate crater collapse, thus explaining the overall shallower depths of mare craters and the transition from simple to complex crater morphology (i.e., the onset of crater collapse) at smaller diameters as compared to highland craters (Osinski et al. 2019).

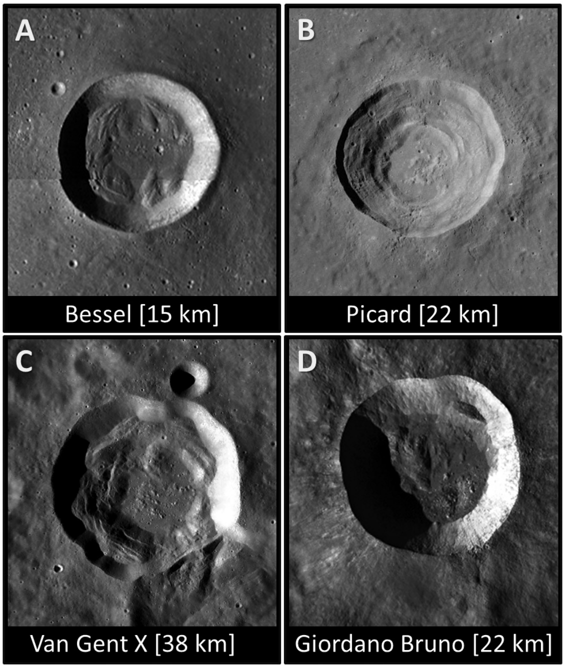

Figure 5. Images of transitional lunar impact craters. **A, B)** Transitional craters in mare targets (Bessel, Picard). **C, D)** Transitional craters in highland targets (Van Gent X, Giordano Bruno). Images: Portions of LROC WAC mosaics (NASA/GSFC/Arizona State University).

Numerical modeling of lunar transitional craters also suggests that variations in impact velocity and/or target porosity could result in smaller or larger than expected diameters (Silber et al. 2017), potentially accounting for some of the observed morphological differences, particularly among craters formed in similar target rocks. Moreover, since the melt production is sensitive to both impact velocity (Wünnemann et al. 2006, 2008) and target porosity (Pierazzo et al. 1997), these two parameters could provide observational means to discern between craters produced by small/fast and large/slow impactors (Silber et al. 2018).

4.3. Complex craters

Gilbert (1893) observed that a crater's floor becomes flatter and a topographic high appears in the center as the crater diameter increases (Fig. 2B). Early studies of terrestrial craters revealed that above a certain size threshold, rocks in the crater center are stratigraphically uplifted with respect to their pre-impact position (Dence 1964). The presence of a central topographic high in lunar craters, combined with these observations of craters on Earth, was subsequently used to define the term *complex impact crater* (Dence 1964; Quaide et al. 1965). Complex craters have smaller depth-diameter ratios than simple craters, of ~1:10 to 1:20 (Figs. 3B, 4) (Pike 1977). In addition to having much shallower depths, complex craters exhibit more complicated features, including an elevated and fault-terraced rim, a relatively flat interior (also referred to as the "annular trough"), and an uplifted central topographic high (Figs. 2B, 3B). Early studies of terrestrial craters demonstrated that the presence of a relatively flat interior is due to infilling by allochthonous crater-fill deposits (comprising a mix of impact breccias and impact melt rocks) (Dence 1964, 1972; Grieve et al. 1977); the topography of crater floors underlying these deposits can vary on the km scale within a very short distance. Modern high-resolution imagery of lunar craters showing exquisite flow textures, cooling cracks, and visible clasts in dark-toned deposits, is consistent with these terrestrial observations and with the presence of impact breccias and impact melt rocks in the interior of lunar craters. Recent studies suggest that the elevated rims of complex lunar craters (with respect to the surrounding pre-impact target surface) result primarily from the structural uplift of the target (~70%), whereas the thickness of the ejecta blanket is of subordinate importance (~30%) (Sharpton 2014; Krüger et al. 2017).

Although the transition from simple-to-complex craters occurs at 18.8 km for the global lunar crater population (see above) (Fig. 4) (Krüger et al. 2018), it is important to note that the transition from simple to complex craters is not abrupt and in the 20 to 45 km diameter range, there are both transitional and complex craters (Kalynn et al. 2013; Osinski et al. 2019); it is only at >45 km that all craters are complex. As with simple and transitional craters (see above), there are also distinct differences between complex craters formed in mare versus highlands targets. Kalynn et al. (2013) showed that complex craters in mare targets are shallower than those in highlands targets and that the heights of central peaks of mare craters are, on average, lower than those of highlands craters over the same diameter range and this difference increases with increasing crater diameter. These observations have been explained as being due to a combination of factors. The more fragmented and porous highlands rocks may allow the formation of deeper craters with larger central uplifts compared with those in the mare (Kalynn et al. 2013). In addition, the presence of layering provides pre-existing planes of weakness that facilitate crater wall collapse, thus explaining the overall shallower depths of mare craters (Osinski et al. 2019). Layering also provides an explanation for the generally lower heights of central peaks in complex mare craters, whereby upon formation, an initially larger peak collapses outwards along layer-parallel faults (Osinski et al. 2019), an interpretation borne out by studies of terrestrial craters in sedimentary targets (e.g., Osinski and Spray 2005).

Further insight into the properties of lunar complex craters comes from results of the GRAIL mission (Zuber et al. 2013) in conjuction with the LOLA instrument (Smith et al. 2010). A notable result was the discovery of a relationship between porosity and impact crater size (Soderblom et al. 2015; Bierson et al. 2016). Whereas larger basins experience mantle uplift during collapse of the transient crater, which gives rise to mass excesses and a positive Bouguer anomaly (see below), large complex craters have typically been observed to yield negative Bouguer anomalies (e.g., Innes 1961; Dvorak and Phillips 1977; Pilkington and Grieve 1992). These negative anomalies, which trend toward more negative values with increasing crater diameters (Soderblom et al. 2015; Bierson et al. 2016), have been interpreted as evidence of increased porosity, through a combination of brecciation, dilatancy, and fracturing (see review by Pilkington and Grieve 1992). Subsequent analyses of GRAIL data have refined this interpretation, noting that short-wavelength gravity data are consistent with relatively low porosity in the uppermost kilometer of a crater floor (Venkatadri and James 2020; Wahl et al. 2020). Near-surface reductions in porosity may be explained by melting or thermal closure of pore spaces associated with an impact event. A trade-off between the creation and destruction of porosity is evident in diameter-dependence of a crater's gravity signature: smaller complex craters (<35 km diameter) tend to yield a positive Bouguer anomaly, which suggests that the closure of pore spaces was prominent in the associated impact events (Milbury et al. 2015; Soderblom et al. 2015). This tradeoff between porosity creation and porosity destruction has also been explored by numerical modeling of impacts into porous targets, which suggests that the net change in porosity associated with the formation of complex craters depends on the pre-existing porosity (e.g., Milbury et al. 2015).

As described above, it is clear that complex craters play a critical role in the creation and destruction of porosity in the lunar crust. Correspondingly, the presence of pre-existing porosity in the crust regulates the morphology of complex craters. Numerical and experimental studies have shown that porous targets result in reduced crater volumes relative to non-porous rocks (Kenkmann et al. 2018). Impact melt also appears to be more common in the relatively porous highlands (Neish et al. 2014; Stopar et al. 2014), which could be explained by localized amplification of shock pressures at cracks and pores (Güldemeister et al. 2013).

4.4. Peak-ring basins

At a rim diameter of ~200 km, interior rings replace central peaks and impact basins form (Fig. 2C); although the terms *basin* and *crater* can be viewed as being interchangeable. Impact basins are defined as having two (*peak-ring basins*) or more (*multi-ring basins*; described in the next section; Fig. 2D) concentric topographic rings (Hartmann and Kuiper 1962). Transitional structures, called *protobasins* or *central-peak basins* also occur, and possess both a central peak and a peak ring (Pike and Spudis 1987; Stöffler et al. 2006). With improved image, topography, and gravity data provided by recent missions, the number of confidently recognizable rings associated with impact basins has been substantially revised. Updated catalogs based on these new datasets (Baker et al. 2011; Neumann et al. 2015) identify the presence of three protobasins, 16 peak-ring basins, and 11 multi-ring basins. Most of these multi-ring basins have no more than three concentric rings in addition to an inner topographic depression (Neumann et al. 2015). An additional 30 basins have only a single identifiable main ring with no additional rings, and 16 basins are so degraded that they lack visible topographic rings but can be recognized because of their characteristic Bouguer gravity anomaly signatures (Neumann et al. 2015).

Updated and new morphometric measurements of large crater and basin landforms (Baker et al. 2011, 2012; Bray et al. 2012; Kalynn et al. 2013) confirm that the dimensions of central peaks, including their diameters, heights, areas, and volumes increase systematically within rim diameter up to the transition to peak rings. Peak rings have comparatively larger diameters and smaller heights for their rim diameter, suggesting an abrupt transition in the process forming central structures. In the "dynamic collapse model" for the formation of peak rings (e.g., Collins et al. 2002), this abrupt change is predicted to result from the downward and outward collapse of overheightened and gravitationally unstable central peaks. Under that model, the collapsed central-peak material is thrust over the inward-collapsed basin walls to form the peak ring. This process is consistently simulated in sophisticated numerical models of impact-basin formation (Collins et al. 2002, 2008; Kring et al. 2016) and is supported by data from drill cores retrieved from the peak ring of the Chicxulub impact structure (Morgan et al. 2016) and field observations from the Sudbury impact structure (Grieve and Osinski 2020), the only two confirmed peak-ring structures on Earth.

Comparisons between the morphometry of the simulated final basin configurations and lunar morphometric measurements are in general agreement (Baker et al. 2016). However, transitional central structures are currently not well understood, with the models predicting wider central structures than observed at these diameters and a smaller crater-to-basin transition diameter (Baker et al. 2016). An alternative "nested melt-cavity" model (Cintala and Grieve 1998; Head 2010) has been proposed and modified (Baker et al. 2016) that hypothesizes that with increased depth and volume of melting, the column of material that would form a central uplift is liquid and can no longer support a stable central peak. At the size of impact basins, which would have a non-proportionally large volume and depth of impact melting, no central peaks should form and peak rings may be left as the only topographically stable landform (Cintala and Grieve 1998). The model shows some consistency with planetary observations (Baker et al. 2016) but has not been fully tested through numerical modeling and appears at odds with interpretations from the Chicxulub drill cores (Morgan et al. 2016).

The mineralogy of the interior rings of lunar peak-ring basins and multi-ring basins, as inferred from recent hyperspectral imaging from M^3 and other instruments, has been used to constrain the depths of origin of uplifted basin materials. The presence of pure anorthosite in many peak rings (Ohtake et al. 2009; Baker and Head 2015; Kring et al. 2016), the Inner Rook ring of Orientale (Cheek et al. 2013) and other multi-ring basins within the lunar highlands (e.g., Spudis 1993) strongly supports a crustal origin for a large fraction of basin inner-ring material. Comparisons with estimates of the maximum depth of excavation, GRAIL and LOLA-derived crustal thickness, and numerical modeling all constrain the depth of origin of peak-ring material to near 0.1–0.12D (Collins et al. 2002; Baker and Head, 2015; Baker et al. 2016; Kring et al. 2016). In addition, numerical models predict that the peak rings should be composed of crustal rocks recording a range of peak shock pressures (Kring et al. 2016; Morgan et al. 2016), explaining the presence of crystalline plagioclase that may not have been shocked above 25 GPa. These estimates for the depth of origin of peak rings are dramatically different from previously inferred depths of origin of central peaks, which previous researchers had estimated using the maximum depth of melting (Cintala and Grieve 1998; Tompkins and Pieters 1999; Cahill et al. 2009). If applied to impact basins, the maximum depth of melting would imply mantle-derived material, which is inconsistent with the observed mineralogy and models of peak-ring formation.

4.5. Mascons and multi-ring basins

The earliest orbital observations of the Moon discovered surprisingly large (> 500 mGal) positive gravity anomalies (Muller and Sjogren 1968), produced by mass concentrations or "mascons" closely associated with the large impact features described as multi-ring basins that are often flooded with mare lava flows (Fig. 2D). The discovery of mascons led to the development of two main endmember theories for their formation. The first hypothesis was that post-impact resurfacing by mare volcanism, with higher density than the surrounding crust, created large surface loads, evidenced by extensional tectonic features (Solomon and Head 1979). However, the average thickness of mare is typically <1 km (e.g., Gong et al. 2016) and only a few areas surrounding Imbrium have sufficiently thick deposits of mare (>2 km) to generate the observed gravity highs. Furthermore, the considerable gravity anomalies associated with the Orientale Basin could not be successfully modeled solely by surface loads (Zuber et al. 2016). The mascons thus represent a crustal state out of isostatic equilibrium that is preserved in the lithosphere after large impact events.

Bouguer gravity anomalies (corrected for surface topography) are invariably positive over the central portions of peak-ring and multi-ring basins (e.g., Baker et al. 2016). Inversions of gravity using one or more crustal layers (Wieczorek et al. 2013) support the second hypothesis for mascon basins, which is the role of uplifted mantle in producing the gravitational signature of the majority of known basins. Such inversions showed as well that the central region of thinned crust is surrounded by a collar of thickened crust. Johnson et al. (2016) proposed that this collar develops as part of crustal flow during the collapse of the transient crater. The initially sub-isostatic state of the basin center later undergoes a process of viscous relaxation over much longer time scales, whereby the lithosphere over the collar is mechanically coupled to the basin center and flexurally supports the mass of the uplifted mantle, contributing the bulk of the mascon free-air gravity high (Andrews-Hanna et al. 2013), supplemented by cooling and volcanic fill (Melosh et al. 2013). The South Pole-Aitken (SPA) basin, the Moon's largest impact basin, is so large and the Moon was so warm and weak at the time of its formation that no mascon could form during the basin's relaxation (Trowbridge et al. 2020).

New insight into the structure of multi-ring basins resulted from the GRAIL Extended Mission, which targeted Orientale at 3–5 km spatial resolution (Zuber et al. 2016). Gravity maps produced from these observations revealed that at least 3.4×10^6 km^3 of material were redistributed by the basin-forming impact and the transient crater had a diameter of 320–460 km. These results support the idea that none of Orientale's observed rings correspond to the transient crater (Johnson et al. 2016; Zuber et al. 2016). GRAIL also revealed that Orientale's outer rings, the Outer Rook and Cordillera (Fig. 2D), are large normal faults that produced offsets at the crust mantle interface (Zuber et al. 2016). A follow up study of Orientale's rings and their gravity signatures supports these conclusions and also clearly shows that Orientale's rings are associated with intrusive ring dikes (Andrews-Hanna et al. 2018). Using the constraints from GRAIL as a guide, Johnson et al. (2016) simulated the formation of the Orientale multiring basin. Their models showed that the inflow of warm, weak material at depth leads to extensional failure of the lithosphere ultimately producing Orientale's outer rings (Fig. 6). Recent simulations over a larger parameter space by Johnson et al. (2018) reproduced the trends in ring spacing as a function of basin size, including the transition from peak-ring to multiring structures. These simulations validate the ring tectonic theory of multiring basin formation (Melosh and McKinnon 1978). Johnson et al. (2016) also showed that the Inner Rook ring formed as the result of the collapse of a central uplift similar to the formation of peak-rings of smaller basins (Kring et al. 2016; Morgan et al. 2016). In these simulations, buoyant crustal material flows to the center of the basin covering the once exposed mantle (Freed et al. 2014; Johnson et al. 2018). This inflow of crustal material to the center of the basin may even occur for the South Pole-Aitken basin (Trowbridge et al. 2020). This may explain why detections of mantle material are not more prevalent inside of large basins without the need to invoke unexpectedly shallow excavation depths.

5. EJECTA DEPOSITS

A defining feature of all hypervelocity impact craters are ejecta deposits (Figs. 2, 3, 5). Despite this, the origin and emplacement of ejecta deposits remains one of the most poorly understood aspects of the impact cratering process. This is due, in part, to the overall low level of preservation of ejecta deposits on Earth. Impact ejecta deposits are better preserved on the Moon, so that recent studies of lunar craters have contributed significantly to our understanding of ejecta deposition.

The definition of impact ejecta is any target material, regardless of its physical state, that has been transported beyond the rim of the transient cavity (Osinski et al. 2012). In simple and transitional impact craters, where collapse of the transient crater rim is minor, enlarging

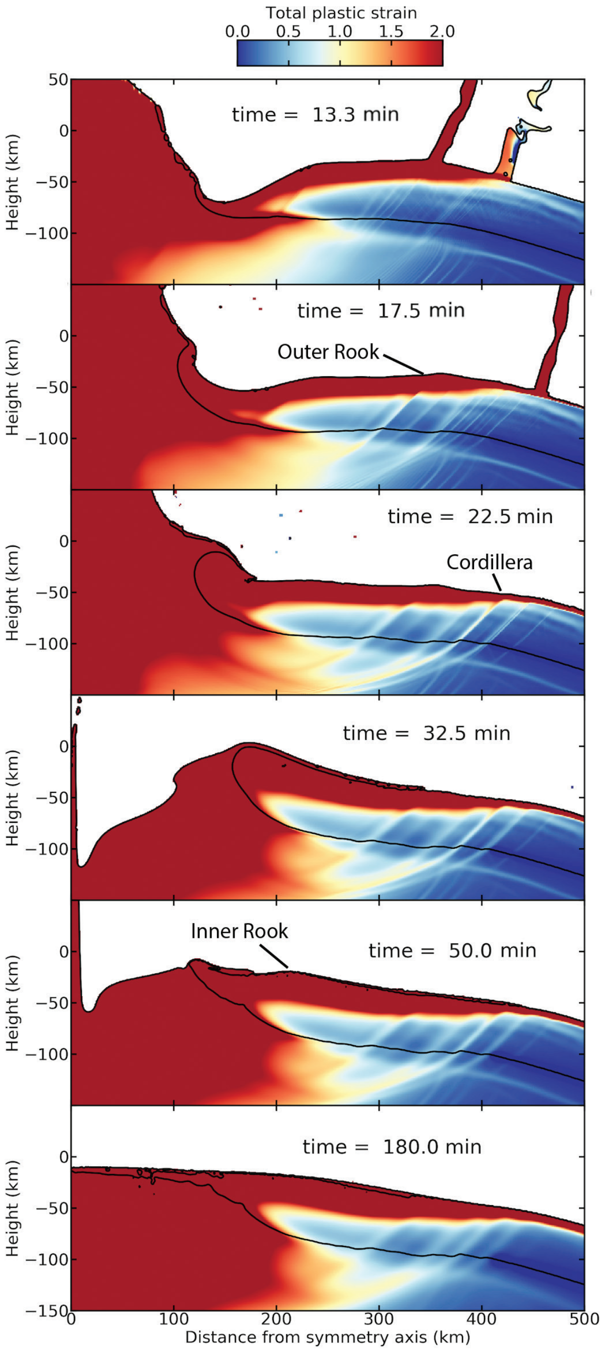

Figure 6. Time series of the formation of the Orientale basin and its rings. Material is colored according to total plastic strain as indicated by the **color bar**. Model is of a 64-km-diameter projectile striking a Moon-like target at 25 km/s. **Black curves** mark material interfaces. The structures corresponding to Orientale's rings are noted in the figure. Modified after Johnson et al. (2016).

the crater diameter by only a small amount, the identification of ejecta deposits is relatively straightforward (Fig. 3A). In complex craters, however, the transient cavity is essentially destroyed during the modification stage, such that ejecta deposits occur interior to the final crater rim on top of the terraces (Fig. 3B). A further distinction is between proximal and distal ejecta deposits, emplaced <5 and >5 crater radii from the point of impact, respectively.

5.1. Proximal ejecta deposits

Fresh impact craters on the Moon, and indeed all the terrestrial planets, are surrounded by a "continuous ejecta blanket" that extends approximately 1 to 2 crater radii (*Rc*) beyond the crater rim (Figs. 2, 3). This continuous ejecta blanket is thickest at the topographic crater rim and becomes thinner outwards. Early studies of lunar craters led to the development of the now widely accepted model for the emplacement of continuous ejecta blankets: ballistic sedimentation and subsequent radial flow (Oberbeck 1975). According to this model, target materials are excavated with some initial velocity and follow a near parabolic flight path, subsequently falling back to the surface, striking with the same, or slightly lower (ballistic) velocity that they possessed upon ejection. Oberbeck (1975) proposed that the innermost ejecta with respect to the point of impact is launched first and with highest velocity; whereas, the outermost ejecta is launched later with lower velocities and so land closer to the crater rim. Subsequent studies of the continuous ejecta blanket at the ~24 km-diameter Ries impact structure, Germany—known as the Bunte Breccia—provided ground-truth support for the ballistic sedimentation model (Hörz et al. 1983).

An important observation from work on the Bunte Breccia was the recognition that ejecta deposits comprise two distinct components: (1) primary ejecta excavated from the initial transient cavity; and (2) local material or "secondary ejecta" incorporated during transport. This secondary ejecta dominates (~69 vol%, average) the Bunte Breccia. Studies of the Bunte Breccia (Hörz et al. 1983) mirrored observations of the ejecta blanket at the smaller 1.2 km-diameter Meteor (Barringer) Crater, USA (Shoemaker 1963), and supported the hypotheses for lunar craters that continuous ejecta deposits comprise predominantly low shock material and are melt-poor to melt-free. Recent analogue field studies at terrestrial craters have reaffirmed support for the ballistic sedimentation model for emplacement of continuous ejecta blankets and confirmed the observation that such deposits, at least in simple and complex craters, are melt-free to melt-poor (Osinski et al. 2005; Maloof et al. 2010; Mader and Osinski 2018). It is worth noting that recent work by Bray et al. (2018) interpreted flow-like features in the continuous ejecta deposits of the 9 km-diameter Pierazzo lunar crater as being impact melt flows. These authors suggested that upon landing, melt became separated from solid ejecta to form the observed flow features, which occur in ~1.5% of the areal extent of the ejecta deposits.

A critical observation, first reported based on Lunar Orbiter images (Hawke and Head 1977), and confirmed with LRO data (Osinski et al. 2011; Neish et al. 2014), is that ponds and flows of impact melt are commonplace *overlying* ballistic ejecta deposits in the terraced crater rim region and continuous ejecta blanket of simple and complex lunar craters (Fig. 6). Recent work has demonstrated that this is also the case for the 960-km diameter Orientale Basin (Morse et al. 2018); the largest flows around Orientale are up to ~400 km long by 150 km wide and occur up to ~1,350 km from the crater center. These melt deposits are, by definition, ejecta. Furthermore, Osinski et al. (2011) showed that the presence of melt-rich deposits overlying continuous ejecta deposits occurs on all the terrestrial planets. These layers range from patchy to semi-continuous and occur inside and outside the final crater rim overlying the continuous ejecta blanket at both simple and complex craters. The properties of these melt-rich deposits are described in below.

The simplest explanation is that impact ejecta emplacement is a multi-stage process, whereby following the emplacement of a continuous ejecta blanket through ballistic sedimentation and radial flow (Oberbeck, 1975) during the excavation stage of crater formation, a second major phase of ejecta emplacement occurs at the end of the excavation stage and into the modification stage (Osinski et al. 2011) (Fig. 1). This later phase takes the form of ground-hugging impact melt-rich flows that move out of the transient cavity and up to, and often over, the rapidly evolving crater rim (Fig. 1). Examination of impact melt surrounding complex craters on the Moon indicates pre-impact topography often controls the final resting place of this melt, with deposits found preferentially outside of rim crest lows (Neish et al. 2014). There is also evidence for limited ballistic emplacement of impact melt, with evidence for melt being ejected both close to the crater rim (Bray et al. 2018) as well as much further afield (Robinson et al. 2016).

Radar observations of lunar craters have revealed the existence of yet another layer or facies of impact ejecta: namely halos of rock-poor material ("radar-dark halos") extending to a distance of ~2 crater radii beyond the continuous ejecta blanket (Schultz and Mendell 1978; Ghent et al. 2016). These halos are apparent in observations at both P- and S-band radar and show spatially coincident and sharp outer boundaries at both wavelengths, indicating that radar-dark halos represent deposits on the order of a meter thick (Ghent et al. 2010). The current hypothesis for emplacement of this volumetrically significant impact facies is a combination of ballistic sedimentation (see above) and granular flow associated with the advancing ejecta curtain, which causes comminution of all pre-existing regolith materials to a distance controlled by the total energy and momentum contained within the ejecta curtain (Ghent et al. 2016).

Lunar cold spots are related features distinguished by anomalously cold nighttime surface temperatures surrounding young craters (Bandfield et al. 2014). Revealed by thermal images from the Diviner Lunar Radiometer Experiment, cold spots typically have inner margins that start a few *Rc* from the rim, and extend to ~10–100 *Rc*. Several thousand of these features have been identified on the Moon (Hayne et al. 2017; Williams et al. 2018). Notably, their cold temperatures cannot be readily explained by the emplacement of an insulating ejecta layer, because the volume of material implied by the thermophysical anomaly is much larger than the crater's excavation volume.

In the proximal ejecta of cold spot craters, layered deposits consist of high-albedo, optically immature material. High-resolution LROC images show that the morphology and layering of the continuous ejecta is consistent with overlapping granular flows (Bandfield et al. 2014). Distal patterns in cold spots are more ray-like and discontinuous. Granular flow and ballistic sedimentation (Oberbeck 1975) may therefore be responsible for "fluffing up" (i.e., decreasing the thermal inertia) of the regolith over great distances to produce cold spots. Based on measurements of their optical maturity, cold spots are among the youngest impact craters on the Moon. Indeed, comparison of their cumulative size frequency distribution (CSFD) with crater production models, along with crater counts of superposed craters on their ejecta, constrains the cold spot retention age to be ~0.5–1.0 Myr (Williams et al. 2018). Observations therefore suggest that all lunar craters may initially have cold spots, which gradually fade due to compaction and settling.

The combined analysis of Diviner rock abundance and radar data allows discrimination of surface from subsurface ejecta rocks. This approach has revealed that ejecta rocks lying on the lunar surface become undetectable to Diviner—by being broken up by small bolides or thermal fragmentation to sizes smaller than approximately one meter, or being covered by fine-grained regolith, or a combination—on a timescale of ~1 Gyr (Ghent et al. 2014). An important consequence of this interpretation is that craters whose ejecta show surface rocks are for the most part Copernican in age, thus providing a straightforward method for identifying the youngest large craters on the Moon for further study. Rocks that appear in radar observations but not in Diviner rock abundance data are buried beneath a centimeter-to meter-scale thickness of fine-grained, thermally insulating regolith. These rocks persist for much longer, perhaps more than 3 Gyr (Ghent et al. 2016), thereby providing a limit on the rate of regolith overturn at various depths. In addition to the total survival time of surface rocks, Diviner data have revealed a robust correlation between the rock abundance of a given crater's ejecta and the crater age (Ghent et al. 2014). This relationship provides a new means of determining the ages of Copernican craters with diameter > 10 km. Applying this relationship, Mazrouei et al. (2019) have documented evidence for a factor of 2–3 increase in the flux of impactors at ~290 Ma on both the Moon and Earth.

5.2. Self-secondary cratering

Recent work involving crater-counting of small diameter craters (<500 m) on the continuous ejecta blanket of Copernican-aged craters show discrepancies in crater size–frequency distributions (CSFDs) between melt units and nearby ejecta (Plescia and Robinson 2011; Hiesinger et al. 2012; Zanetti et al. 2017). Although this discrepancy was noted as long ago as the Surveyor 7 mission at Tycho Crater (e.g., Shoemaker et al. 1969), the abundance of high-resolution imagery from LROC NAC has allowed for more detailed counts and at more Copernican-aged craters (e.g., Aristarchus, Cone, Giordano Bruno, Jackson, King, and others). The results of crater-counts on ejecta blankets are of broad significance because CSFDs are currently the only way to assess an "absolute model-age" for individual impact events (see Hiesinger et al. 2023, this volume). The nature of these discrepancies remains an open question. The two leading hypotheses relate to the differing target properties of melt and ejecta (e.g., Hiesinger et al. 2012; van der Bogert et al. 2017), or to a population of craters on the continuous ejecta formed by late-arriving fragments from the parent crater, so-called self-secondary craters (e.g., Plescia and Cintala 2012; Zanetti et al. 2017). For small craters (where strength dominates) and for the same impactor mass and speed, craters forming on hard, competent surfaces (e.g., impact melt rock) will have relatively smaller diameters whereas craters forming on less competent surfaces (e.g., ballistic ejecta deposits) will have relatively larger diameters. Thus, melt units would "appear" younger than nearby ejecta facies based on the calculation of absolute model ages from CSFD measurements.

The discrepancy could, therefore, be accounted for with a correction factor that accounts for the relative difference in strength between the lithologic units (e.g., van der Bogert et al. 2017, and references therein). However, detailed crater counts over large areas of the ejecta blankets at Aristarchus and Tycho Craters by Zanetti et al. (2017) showed that the crater density (irrespective of crater diameter) is variable within the continuous ejecta blanket and increases radially away from the parent crater rim. Further population differences between adjacent melt and ejecta units of equal area showed that melt units can contain at least 30% fewer craters, suggesting that target property effects on absolute model ages cannot fully account for the discrepancy (Zanetti et al. 2017). Moreover, a lower density of crater occurrence was observed to be correlated with areas of impact melt ponds and flows, suggesting possible erasure or resurfacing of craters formed on the ejecta blanket prior to or during the emplacement of the impact melt facies. For this to occur, late-arriving fragments from the parent impact formation, delayed by enough time for the main-ejecta to be emplaced, and possibly following high-angle trajectories, would have to impact on the newly-formed ejecta-blanket pre- or syn- emplacement of the melt. While late-arriving, high-angle, self-secondary ejecta fragments might be conceptually simple, it is somewhat incompatible with the dynamics of ejecta blanket emplacement as relatively low-angle ballistic trajectories and as an essentially contiguous curtain. Further work is required on this topic and for more information on crater chronology see Hiesinger et al. (2023, this volume).

6. IMPACTITES: THE PRODUCTS OF IMPACT EVENTS

The pressures and temperatures experienced during the impact cratering process result in the vaporization, melting, shock metamorphism, and/or deformation of a substantial volume of the target sequence. The transport and mixing of these variably impact-metamorphosed rocks and minerals during the excavation and modification stage of crater formation produces a wide variety of products, termed *impactites*. Stöffler and Grieve (2007) define impactites as "a collective term for all rocks affected by one or more hypervelocity impact(s) resulting from collision(s) of planetary bodies".

6.1. Shock metamorphism

As described previously, the increase in internal energy accompanying shock compression and subsequent rarefaction during the contact and compression stage of crater formation results in a unique set of irreversible deformation effects, referred to as shock metamorphism (see reviews by Ferrière and Osinski (2012) and French and Koeberl (2010)), as well as melting (see review by Osinski et al. (2018) and also below) and/or vaporization of a volume of target material close to the point of impact. At low shock pressures (~2 GPa), the most characteristic shock metamorphic phenomena, and the only macroscopic indicator of shock, are shatter cones (French and Koeberl 2010). They consist of striated conical to curvi-planar fractures that typically occur in hierarchical networks. Shatter cones are most commonly found in situ within central uplifts of complex craters, but are also found as clasts in dikes intruded into crater floors and in proximal and distal ejecta deposits (Osinski and Ferrière 2016). They are best developed in fine-grained lithologies, but can also be observed—albeit more poorly developed—in coarser-grained lithologies. They should, in theory, be present on the Moon as shatter cones are found in basalt and anorthosite in terrestrial craters (Baratoux and Reimold 2016).

Microscopic shock metamorphic effects are best studied and constrained for quartz, for which there is a well-documented progression with increasing shock pressure. The most commonly observed microscopic shock effects are planar fractures (PFs) and planar deformation features (PDFs) (e.g., Stöffler and Langenhorst 1994; Grieve et al. 1996). Planar deformation features in quartz appear at ~5–10 GPa and extend up to shock pressures of ~35 GPa. At higher shock pressures (>35 GPa), diaplectic glass forms by solid-state transformation, i.e., without melting (Stöffler 1972; Stöffler and Langenhorst 1994). A range of other minor shock features, such as kink bands, mosaicism, and feather features, are also known (French and Koeberl 2010). Shock effects in minerals relevant to the Moon (i.e., plagioclase and pyroxene) are less well understood; however, numerous recent studies have investigated shock effects in plagioclase, via experiments and laboratory studies of Apollo samples, lunar meteorites, and anorthosite from terrestrial impact craters.

While planar fractures and PDFs have been proposed to form in plagioclase (French and Koeberl 2010), recent studies of shocked anorthosite from the Mistastin Lake impact structure, Labrador (Pickersgill et al. 2015b; Xie et al. 2020), and Apollo samples (Pickersgill et al. 2015a), have failed to document any unequivocal PDFs. Various reasons have been suggested for this, including misidentification (microlites, twin planes, and exsolution lamellae can easily be mistaken for PDFs), structural controls relating to the crystal structure of different feldspars, and/or the presence of existing planes of weakness in the form of twin and cleavage planes. Further studies are warranted on this topic.

In plagioclase, the most characteristic shock effect is the transformation to diaplectic glass (also referred to as "maskelynite"), which has generally been assumed to occur at ~20–35 GPa (French and Koeberl 2010). Recent work, however, has recognized that the exact conditions required to transform plagioclase to maskelynite are highly dependent on multiple factors including pressure, temperature, composition, and strain rate (Fritz et al. 2017; Jaret 2018), which may limit our ability to use the presence of shocked plagioclase to determine precise impact conditions. Still, the progression of effects can be seen optically and with more quantitative analytical techniques such as Raman and infrared spectroscopy (Jaret et al. 2015; Martin et al. 2017; Jaret 2018; Xie et al. 2020), X-ray diffraction (Pickersgill et al. 2015a), and cathodoluminescence (Kayama et al. 2012).

Intriguingly, it has long been noted that diaplectic glass is rare in Apollo samples (Chao et al. 1971). Rubin (2015) most recently summarized the data on diaplectic glass in basaltic Apollo samples, concluding that the proportion of diaplectic glass-bearing lunar basalts is ~1%. The same holds for lunar anorthosites. For example, Fernandes et al. (2013) found no diaplectic glass among 12 anorthositic Apollo 16 rake samples. Xie et al. (2017) studied a large suite of anorthosite samples from all the Apollo missions by optical and Raman spectroscopy and similarly found no plagioclase grains fully transformed to diaplectic glass; although partial transformation was noted in several samples. In contrast, diaplectic glass has been reported from approximately one-third of lunar basaltic meteorites (Rubin 2015) and lunar meteorites generally show a higher level of shock than Apollo samples (Pernet-Fisher et al. 2017) (see also Joy et al. 2023, this volume). This observation has been explained as potentially being due to sampling biases and reflect either differences in collection, given that lunar meteorites were ejected from the Moon by impacts whereas Apollo samples were not. Alternatively, this could be a location bias, where lunar meteorites represent a more global sampling (Joy et al. 2023, this volume); whereas Apollo samples come from a restricted area of the lunar nearside.

Aside from the slight differences between lunar meteorites and Apollo samples, the level of estimated shock is generally higher than interpretations based on remote spectroscopy (Martin et al. 2017; Pernet-Fisher et al. 2017), with the latter suggesting the presence of shocked plagioclase interspersed with crystalline plagioclase outcrops at a scale of few hundred meters (Dhingra et al. 2011; Donaldson Hanna et al. 2014). Reconciling these differences between samples and remote analyses remains an important issue for future studies.

In contrast to plagioclase, there has been little recent work on shock effects in pyroxene. Nonetheless, a range of shock effects have been identified, including mosaicism, PDFs, and mechanical twins (e.g., Rubin 1997; Langenhorst 2002). The SiO_2 high pressure minerals coesite and stishovite were discovered as micro-inclusions in amorphous silica grains in shocked melt pockets of the lunar meteorite Asuka-881757 (Ohtani et al. 2011) suggesting that high-pressure impact metamorphism is a common phenomenon in the brecciated lunar surface, which has been altered by the heavy meteoritic bombardment.

6.2. Impactites

Much of our knowledge of impactites comes from studying terrestrial impact craters where context is known and ground truth is possible. The most widely used classification scheme is that proposed by a study group as part of the IUGS Subcommission on the Systematics of Metamorphic Rocks (Stöffler and Grieve 2007). This group recommended that impactites from a single impact be classified into three major groups: *shocked rocks*, *impact melt rocks*, and *impact breccias*. However, it is important to note that the nomenclature of impactites remains an ongoing topic of discussion with the terrestrial impact cratering community, particularly for impact breccias that contain some portion of "melt" (e.g., Osinski et al. 2008, 2016). Notably, the framework for the IUGS classification scheme was developed in the early 1990's and remained little changed up to its publication in 2007, despite several major discoveries and advancements in our understanding of impactites. A key advancement has been the ability to go beyond optical microscopy and to image and analyze impactites—which are inherently heterogeneous in nature—at the micron scale using modern scanning electron microscopy and electron microprobe analysis. A notable example is that the first detailed SEM study of "suevite" from the Ries impact structure, Germany—the type locality for this impactite type—was not published until the 21st century (Osinski et al. 2004). Based on this and other SEM studies, an alternative, more descriptive nomenclature for impact melt-bearing impactites has been proposed (Osinski et al. 2008). For the Moon, an additional complication is that impactites may be generated from multiple impacts, hence, Stöffler and Grieve (2007) proposed two additional impactite groups: *impact regolith* and *shock lithified impact regolith*. The following subsections reflect current thinking regarding impactites of any parent body, including the Moon.

6.2.1. Shocked rocks. Shocked rocks are the simplest impactite group to understand. They are non-brecciated, melt-free rocks displaying unequivocal effects of shock metamorphism (see see separate section above). Given the intensity of impact cratering on the lunar surface it is likely that most non-brecciated, non-melted lunar rocks would fall into this category.

6.2.2. Impact melt rocks. One of the most characteristic outcomes of hypervelocity impact is the melting of a substantial portion of the target sequence (see review by Osinski et al. 2018), with the volume of melt increasing differentially with increasing crater size (Cintala and Grieve 1998). The major reason for this is that cratering efficiency decreases with increasing crater size such that the volume of impact melt with respect to the volume of the transient cavity increases (Grieve and Cintala 1992). The result is that impact melt volume scales with the size of an impact crater with significantly larger volumes produced at the basin scale (Cintala and Grieve 1998). Several other dependencies are also known including target and impactor composition, porosity, impact angle and impactor velocity (e.g., Pierazzo et al. 1997; Pierazzo and Melosh 2000; Osinski et al. 2008; Wünnemann et al. 2008).

Impact melt rocks are subclassified according to their clast content (i.e., clast-free, -poor, or -rich) and/or degree of crystallinity (i.e., glassy, hypocrystalline, or holocrystalline) (Fig. 7). Although not as well studied or generally acknowledged, igneous rocks formed by hypervelocity impact share many textural similarities with endogenic igneous rocks. Indeed, once solidified, these impact-generated melts satisfy the definition for igneous rocks (Osinski et al. 2018). As such, the common textures of endogenic igneous rocks are applicable and appropriate for describing impact melt rocks, particularly textures reflecting the size of the mineral grains (phaneritic, aphanitic, porphyritic, pegmatitic, and glassy), as well as other properties, such as vesicularity (Fig. 7). It is also clear from studies of craters on Earth that magmatic differentiation of impact melts—i.e., the process whereby a parental magma can evolve, resulting in a range of diversified products (Wilson 1993)—does occur if the volumes of melt are great enough. The best example on Earth is the so-called Sudbury Igneous Complex (SIC), which is the remnant of the coherent impact melt sheet at the Sudbury impact structure, Canada (Grieve et al. 1991). The SIC outcrops at the surface occur as an elliptical body, comprising norite (~25%) overlain by quartz gabbro (~15%) and capped by granophyre (~60%); these rocks are predominantly clast-free. The mineralogy and geochemistry of the SIC support a cogenetic source for these sub-units produced by fractional crystallization of a single batch of silicate liquid (Therriault et al. 2002). The potential for magmatic differentiation of impact melts produced during basin forming impacts (such as South Pole-Aitken and Orientale basins) has been re-evaluated through melt modeling and analysis of recent remote sensing datasets, invigorating debate on the likely contribution of crystalline impact melt to the crustal inventory of rocks (Vaughan et al. 2013; Hurwitz and Kring 2014; Spudis et al. 2014; Vaughan and Head 2014).

Lunar rocks conforming to most of the aforementioned textural impact melt rock types are documented in the literature and, despite a rigorous set of criteria to identify pristine endogenously igneous lunar rocks (Warren 1993), it is tantalizing to think that there may be more lunar impact melt rocks in the Apollo sample collection given the similarities between clast-free to clast-poor igneous rocks of endogenic versus impact melt origin. A case example is Apollo 14 sample 14073, which was originally interpreted as a basalt, but that is now classified as an impact melt rock (Fig. 7). This was only possible through the work of Fagan et al. (2013) and Neal et al. (2015) who developed a method using crystal size distributions to distinguish between endogenic igneous and impact-derived melt rocks. For a comprehensive overview of our current understanding of impact melt rocks, including a discussion of how to determine the origin of extraterrestrial igneous rocks, the reader is referred to Osinski et al. (2018).

When it comes to clast-rich impact melt rocks, there has typically been less debate in the literature about their impact origin. What is not as straightforward, however, is the terminology that has been applied to such rocks. The terms "crystalline melt breccias" and "impact melt breccias" are widely applied to lunar rocks composed of mineral and rock fragments within a crystalline matrix (Stöffler et al. 1980). As the largest population of "breccias" from the lunar highlands, these rocks can exhibit heterogenous textures with the crystalline igneous matrix observed to vary from the fine to coarse grained within the same sample (Stöffler et al. 1980).

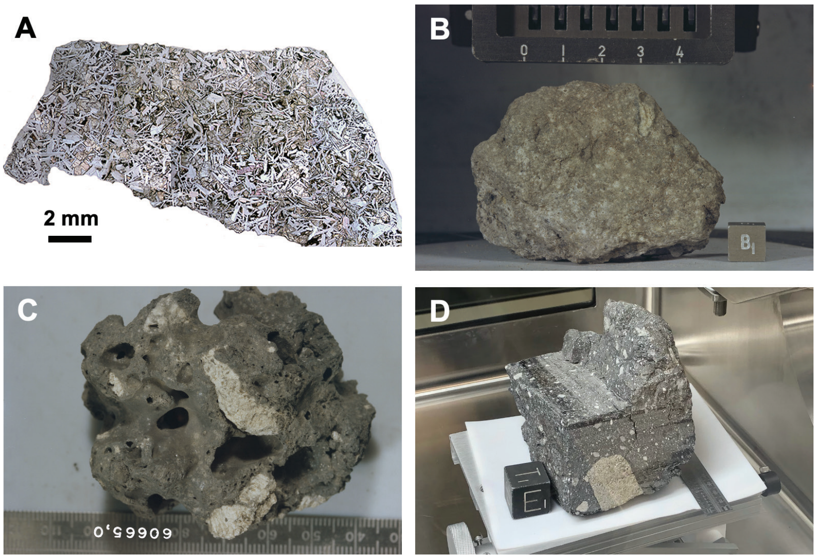

Figure 7. Lunar impactites. **(A)** Apollo 14 sample 14073. Originally interpreted as a basalt, this sample is now classified as an impact melt rock (Neal et al. 2015). **(B)** Aphanitic impact melt rock from the Moon. Apollo 17 sample 73217. Image: NASA. **(C)** Glassy impactite from the Moon. Apollo 16 Rake Sample 60665,0. Image: NASA. (D) Glass-matrix regolith breccia. Apollo sample 15459,0.

Crystalline melt breccias and impact melt breccias are, more accurately, clast-rich impact melt rocks and should be referred to as such according to the IUGS recommendations (Stöffler and Grieve 2007). Similarly, so-called glassy melt breccias, described as having a vitrified matrix typically embedded with minerals and rocks, are simply glassy or aphanitic clast-rich impact melt rocks (Fig. 7). Some lunar glassy melt breccias are clast-free requiring further study to distinguish them from volcanic glass (Stöffler et al. 1980).

Studies of impact melt deposits on the Moon through remote sensing have revealed significant new insights into the emplacement and physical properties of such impactites. One of the most surprising results of these recent missions is the abundance of impact melt deposits on the lunar surface (see Fig. 8), especially around smaller and older craters than previously recognized. Early work suggested that impact melt deposits at small lunar craters were rare (e.g., Hawke and Head 1977); however, a survey of nearly 1,000 simple craters showed that for fresh craters, ~15% of those <300 m in diameter, and 80% between 600 m and 5 km in diameter contain ponded impact melts (Stopar et al. 2014). Pools of impact melt have been recognized on the floor of craters as small as 100 m (Plescia and Cintala 2012).

High-resolution imagery from recent missions has provided detailed views of the structure of the melts, showing evidence for cooling cracks, leveed channels, and inflation features (FIg. 8; Bray et al. 2010)—as with samples, all features characteristic of endogenic igneous rocks. These observations suggest that impact melt remains liquid on the lunar surface over longer timescales than previously thought. This is supported with the work of Denevi et al. (2012), who proposed that lunar impact melt flows have lower viscosities and higher temperatures than terrestrial lava flows, consistent with observations from terrestrial craters that impact melts are superheated to temperatures >2,450 °C (Grieve et al. 1977; Timms et al. 2017; Osinski et al. 2018), a finding that has recently been confirmed for lunar impact melts (White et al. 2020). Indeed, there is evidence for potentially large-scale mobility of impact melt in the form of planar melt sheets or wavefronts (e.g., Dhingra et al. 2017) and flows (e.g., Dhingra et al. 2013) inside lunar craters (Figs. 8C, D, G). The use of M^3 spectral data also led to the detection of a mineralogically distinct, sinuous impact

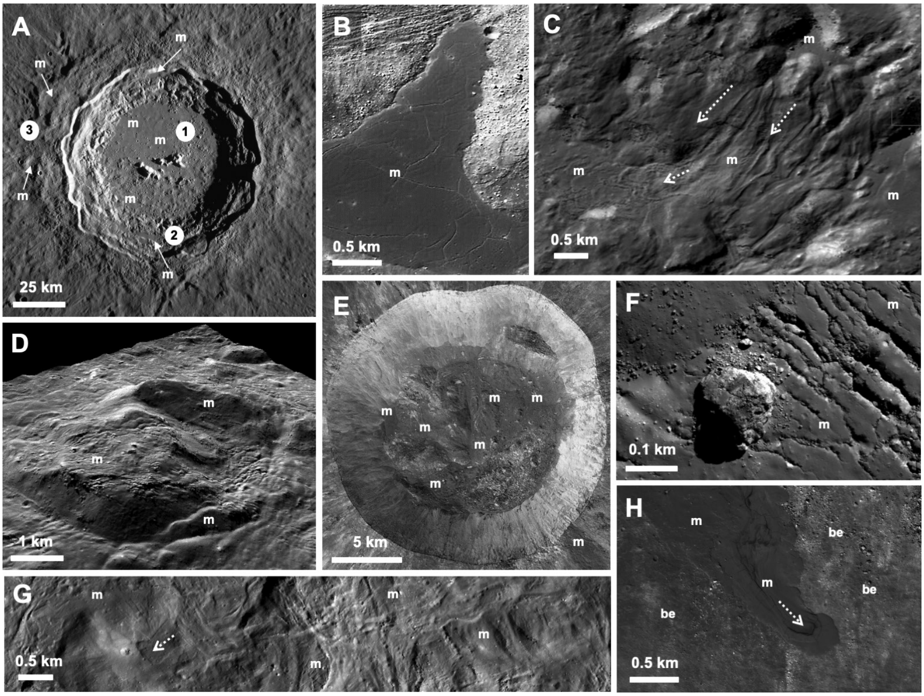

Figure 8. Impact melt deposits ("m") within and around lunar impact craters. **(A)** LROC WAC mosaic of the Copernicus crater (9.6°N, 20.1°W; 96 km diameter), which has deposits of impact melt ("m") on its floor **(1)**, terraces **(2)**, and outside the rim **(3)**. The melt deposits on the terrace and outside of the rim constitute proximal ejecta deposits (see section 5.1) (NASA/GSFC/Arizona State University). **(B)** Kaguya TC image of a melt pond beyond the rim of Tycho crater (43.3° S, 11.3° W; 85 km diameter). Note the distinctive cooling cracks and difference in the surface morphology with respect to the surrounding ballistic ejecta deposits. **(C)** Impact melt deposits on the wall of Tycho crater. Melt can be seen to have ponded and then flowed downhill (**dashed arrows**). **(D)** Impact melt deposits on the floor of Jackson crater (22.04°N, 163.32°W; 71 km diameter) completely draping a massive boulder (>1 km), potentially related to the central peaks. Note the melt veneer breaking-off at the edges. **(E)** LROC NAC mosaic of the Giordano Bruno crater (32.96° N, 102.9°E; 22 km diameter). Impact melt partially covers the floor of this transitional impact crater (NASA/GSFC/Arizona State University). **(F)** Fractured impact melt deposits located on the top of the central peak at Tycho crater. Note the boulder clast (~1 m) resting on the melt. Portion of LROC NAC image M127008391L (NASA/GSFC/Arizona State University). **(G)** Kaguya TC image of impact melt draped floor of Jackson crater (northern section). Note the chaotic melt movement in all directions indicated by an arrow and wide lobes (around the letter '**m**'). The entire region is part of a slightly raised platform above the floor. **(H)** Impact melt flow on the southern rim of Giordano Bruno crater. The melt flow clearly overlies ballistic ejecta deposits ("be") in this NAC image (NASA/GSFC/Arizona State University). Source images for Tycho and Jackson impact melt deposits are TCO_MAP_02_S42E348S45E351SC and TCO_MAP_02_N24E195N21E 198SC, respectively. Images B) and C) are adopted from Dhingra (2015). Images D) and G) are modified from Dhingra et al. (2017).

melt feature at Copernicus crater that possesses no detectable morphological signature (Dhingra et al. 2013), which potentially necessitates a shift from morphology-only basis for describing impact melt flows. The latter finding also documented large-scale mineralogical heterogeneity within impact melt for the first time on the Moon, which has important implications for impact-melt mixing in the case of heterogeneous target rocks.

The Mini-RF radar on LRO has also enabled the identification of previously unrecognized impact melt flows, around older and more degraded impact craters (Carter et al. 2012). Mini-RF is an S-Band (12.6 cm) radar capable of penetrating up to a meter through the lunar regolith, allowing for the detection of buried melt deposits. Impact melt flows are easy to detect at radar wavelengths because they are extremely rough at the centimeter to decimeter scale. The reason for this roughness is unclear, but it may relate to the unusual cooling conditions that the melts are exposed to on the lunar surface (Neish et al. 2017). These radar observations allowed for the first global inventory of lunar impact melts to be compiled since that of Hawke and Head (1977). The observations suggest that impact melt is more common in the highlands than the mare, that the smallest craters have the longest melt flows relative to their size, and that most lunar complex craters have melt that escaped the crater interior via the lowest point in their rim (Neish et al. 2014).

A final important point regarding impact melt rocks is that they are the main means by which impact events can be dated (Jourdan et al. 2009). As age dating techniques have achieved higher precision, impact melt rock, whether clast-rich or clast-poor, has been essential in understanding the bombardment rate (e.g., Hartmann et al. 2007; Puchtel et al. 2008; Michael et al. 2018), the accretionary history (e.g., Puchtel et al. 2008; Gleißner and Becker 2017), and crustal accumulation (e.g., Norman et al. 2016) for the Moon. The recognition of impact melt-bearing samples and being able to distinguish them from volcanic products is, thus, important for future robotic and/or human sample return missions.

6.2.3. Impact breccias. Impact breccias are, arguably, the most common impactite produced during hypervelocity impact events. According to Stöffler and Grieve (2007), impact breccias can be further classified according to the degree of mixing of various target lithologies and their content of melt particles. There have been numerous terms given to impact breccias over the past few decades but the preferred two sub groupings are monomict and polymict impact breccias. The latter are then subdivided into *lithic impact breccias*, which are melt free, and so-called “suevite”, which contains cogenetic impact melt particles (Stöffler and Grieve 2007). It has been pointed out, however, that there are significant inconsistencies with the application of the term “suevite” in the literature (Grieve et al. 1977; Grieve and Therriault 2012) and that some variants are more accurately categorized as impact melt rocks (e.g., Osinski 2004; Sapers et al. 2014), while others may not even be primary impactites but rather sedimentary rocks or impact equivalents of volcaniclastic rocks (e.g., Osinski et al. 2020). The term *impact melt-bearing breccia* offers an interim solution until the nomenclature issues of terrestrial impactites are resolved.

The term fragmental breccia has been applied to an impactite composed of clastic rock debris derived from different lithologies of variable composition, texture, and degree of shock (Stöffler et al. 1980). From this, two subclasses were originally defined. One type was observed to contain impact melt particles, which have similar chemical composition and could potentially be cogenetic. These samples have been proposed as lunar equivalents to terrestrial impact melt-bearing breccias (Chao 1973; Stöffler et al. 1979; Norman 1982). The second type is free of cogenetic melt particles and have been equated to clastic breccia layers of the ejecta blanket of terrestrial impact craters (Stöffler et al. 1980). This class of fragmental breccia conforms to the definition of a lithic impact breccia as per the IUGS classification scheme (Stöffler and Grieve 2007) and this is the preferred modern nomenclature.

6.2.4. Impact regolith and shock lithified impact regolith. As noted above, on the Moon, perpetual bombardment over the past 4.5 Ga results in impactites derived from multiple impact events. Stöffler and Grieve (2007) subdivide this class into two groups: *impact regolith*, which is essentially unconsolidated clastic impact debris; and *shock lithified impact regolith*, which as its name implies, is clastic impact debris consolidated by the impact process (Fig. 7D). In this classification, there is a further subdivision of *shock lithified impact regolith* into *regolith breccias* (i.e., with melt either in the matrix and/or as clasts) and *lithic breccias* (i.e., melt-free). It is generally assumed that regolith breccias form from material from the upper few meters of the lunar surface; whereas lithic breccias contain material derived from 100’s m to km’s depth.

Stöffler and Grieve (2007) further note that the term lithic breccia is synonymous with the term *fragmental breccia* introduced by Stöffler et al. (1980). The literature and nomenclature are thus confusing as both lithic and fragmental breccias may have been applied to impactites derived from single and multiple impact events. Nonetheless, the study of fragmental and regolith lunar meteorites have provided a means by which the lithological and geochemical diversity of the lunar crust has been examined (see Joy et al. 2023, this volume). For example, given the interpretation that regolith breccias contain material derived entirely from the upper few meters of the lunar regolith, several recent studies have attempted to use satellite data to constrain the potential source regions of lunar meteorites (e.g., Joy et al. 2010; Robinson et al. 2012; Calzada-Diaz et al. 2015). Regolith breccias thus provide a tool for examining a statistically representative population of the crust and studying the diversity of the regolith outside of the Apollo sample collection.

Thanks to the renewed robotic exploration of the lunar surface, new observations on the role of impacts in forming the lunar regolith have been provided, most notably by the Yutu-2 rover of the Chang'E-4 spacecraft. In addition to the typical small hypervelocity impact craters in the landing site region, Lin et al. (2020) reported many meter-sized shallow pits lined with small glassy fragments, which would conform to the definition of regolith breccias. These authors interpreted these small craters as small secondary impacts formed at low velocity (<~2 km/s), with the glass-rich fragments representing the disaggregated regolith breccia projectiles "excavated from the impact melt-conglutinated and consolidated walls and bottoms of preexisting small craters within the regolith". For a detailed overview of the characteristics and formation of the lunar regolith, see Plescia et al. (2023, this volume).

6.2.5. Impact glass. As noted above, glass is a constituent of some lunar impact breccias and, more rarely, in impact melt rocks (Fig. 7C). A much more common setting for "impact glass" on the Moon, however, is dispersed within the regolith. These glasses are small, ranging from ≤25 μm (e.g., Keller and McKay 1992) to ~6 mm (e.g., Ryder et al. 1996), and, as a result of frequent impact events, both temporally and spatially, are abundant in the lunar regolith. With a variety of compositions (e.g., basaltic, noritic, and feldspathic; Delano 1986), lunar impact glasses can provide compositional information about local and regional areas of the Moon and their $^{40}Ar/^{39}Ar$ ages place constraints on the impact history of the Earth–Moon system (e.g., Gombosi et al. 2015; Zellner and Delano 2015). Impact glasses are found as both fully formed shapes (i.e., spheres, dumbbells, teardrops) and as fragments (i.e., broken shards).

There are three fundamentally different formation mechanisms for "impact glass"—vaporization, melting, and solid-state (i.e., diaplectic glass; see above) (Osinski et al. 2018). Although melting is the most common mechanism, there are three possible paths and products: 1) *Mineral glass* forms via the selective melting of individual minerals and is common in terrestrial impact breccias; 2) *Interstitial impact glass* forms due to localized melting at grain boundaries of minerals and pores; such glasses are found in highly shocked sandstones on Earth (Kieffer 1971) and in meteorites, where they are termed "melt pockets" (Walton and Herd 2007); 3) *Whole rock impact glass* is typically what most workers on terrestrial craters are referring to when they state "impact glass"; these glasses are produced from melting a specific volume of rock that would typically comprise several mineral or rock types (i.e., whole rock melting) (Stöffler 1984).

Lunar impact glasses are generally understood to form as spherical droplets that are subsequently broken into shards during ballistic transport due to high thermal stresses caused by rapid quenching from hyper-liquidus temperatures (Ulrich 1974; Zellner and Delano 2015). There is no consensus on how these impact glasses are produced, but several investigators (e.g., Zellner et al. 2002; Delano et al. 2007; Korotev et al. 2010) have reported that impact-generated glasses commonly have chemical compositions similar to that of the local regoliths in which they are found, suggesting that some lunar impact glasses form by melting a portion of the lunar regolith. This observation is consistent with theoretical modelling, which shows that porous target-materials (such as lunar regoliths with ~37% porosity) generate higher melt volumes than non-porous targets at a given impact energy and that the volumes of impact-generated melt increases with increasing porosity of the target-materials (Wünnemann et al. 2008).

Additionally, there is no consensus as to what size impact craters produce lunar impact glasses. Hörz and Cintala (1997) suggested that impact glasses are formed via micrometeorite impacts into target rocks but it is unlikely that these tiny impacts can be responsible for creating the large volumes of lunar impact glasses (e.g., ~3×10^7 μm^3 for a 400 μm diameter glass spherule) found in the lunar regolith. Glass-lined impact craters were observed on the lunar surface as small as a few meters (Harrison Schmitt, personal communication). Several investigators (e.g., Delano 1991; Delano et al. 2007; Korotev et al. 2010) have found a large portion of impact glasses in different Apollo regolith samples that have compositions different from any mixture of regolith at the Apollo collection site, indicating that these lunar impact glasses were ballistically transported from craters ≥100 km away. A further implication is that these glasses represent distal and proximal ejecta and are, therefore, akin to whole rock impact glasses documented in terrestrial craters (Stöffler 1984; Osinski et al. 2018). Therefore, contrary to the report by Hörz and Cintala (1997), impact glasses of different sizes and shapes are most likely formed in a range of crater sizes (<1 m to >100 km). Theoretical work by Johnson and Melosh (2012, 2014) supports this conclusion; they reported the formation of terrestrial impact spherules with diameters 0.15—2.5 mm, depending on the size of the impactor. Recent work (e.g., Huang et al. 2018) attempts to resolve the issue of how the history (e.g., transportation from one location to another) of lunar impact glasses is affected by regolith gardening.

6.2.6. Agglutinates. Lunar agglutinates are not impact glasses *sensu stricto* but rather are unhomogenized melt produced by the fusion of the finest fraction of lunar soils (F^3 model; e.g., Basu et al. 2002) that contain a complex mixture of glass, mineral clasts, and polymineralic fragments. Agglutinates can form during mid-to-high pressure (18–70 GPa) impacts into lunar soils and gabbro (See and Hörz 1988; Hörz and Cintala 1997) as well as by melting during micrometeorite impact onto small (~100 mm) targets in the lunar soils (Basu and McKay 1985). Details about the competing theories for the formation of agglutinates have been summarized in Basu et al. (2002).

7. CONCLUDING REMARKS

Much has been learned about impact processes on the Moon since the overview by Stöffler et al. (2006) in New Views of the Moon (NVM-1), as shown by the expansion of that single chapter in 2006 into two in the present volume (i.e., *Chronology* and *Impact Features and Processes*). Clearly, asteroidal and cometary impacts have dominated the evolution of the lunar surface since the Moon's formation and they continue to sculpt the landscape that future astronauts, human and robotic, will explore and utilize. A lot of this learning is also of great relevance to other planetary bodies in the solar system. Much of the recent advances in knowledge has come from high-resolution global surveys of the Moon from several recent missions, continuing efforts in the laboratory, field studies at terrestrial crater analogues, and increasingly sophisticated computer simulations of lunar impact processes. We expect (and hope) that the next generation of studies will focus on more localized research of the lunar surface itself as landers and astronauts return to the Moon. Such efforts have already begun with the successful Chang'E 3 and 4 missions with their Yutu rovers, but we expect that this is only the harbinger of much more expanded efforts by multiple nations.

ACKNOWLEDGMENTS

The authors wish to thank the three reviewers for their helpful and constructive reviews of this chapter.

REFERENCES

Ahrens TJ, O'Keefe JD (1972) Shock melting and vaporization of Lunar rocks and minerals. Moon 4:214–249

Andrews-Hanna JC, Asmar SW, Head JW, Kiefer WS, Konopliv AS, Lemoine FG, Matsuyama I, Mazarico E, McGovern PJ, Melosh HJ, Neumann GA (2013) Ancient igneous intrusions and early expansion of the Moon revealed by GRAIL Gravity Gradiometry. Science 339:675–678

Andrews-Hanna JC, Head JW, Johnson BC, Keane JT, Kiefer WS, McGovern PJ, Neumann GA, Wieczorek MA, Zuber MT (2018) Ring faults and ring dikes around the Orientale basin on the Moon. Icarus 310:1–20

Baker DMH, Head JW (2015) Constraints on the depths of origin of peak rings on the Moon from Moon Mineralogy Mapper data. Icarus 258:164–180

Baker DM, Head JW, Fassett CI, Kadish SJ, Smith DE, Zuber MT, Neumann GA (2011) The transition from complex crater to peak-ring basin on the Moon: New observations from the Lunar Orbiter Laser Altimeter (LOLA) instrument. Icarus 214:377–393

Baker DM, Head JW, Neumann GA, Smith DE, Zuber MT (2012) The transition from complex craters to multi-ring basins on the Moon: Quantitative geometric properties from Lunar Reconnaissance Orbiter Lunar Orbiter Laser Altimeter (LOLA) data. J Geophys Res 117: E00H16

Baker DMH, Head JW, Collins GS, Potter RWK (2016) The formation of peak-ring basins: Working hypotheses and path forward in using observations to constrain models of impact-basin formation. Icarus 273:146–163

Bandfield JL, Song E, Hayne PO, Brand BD, Ghent RR, Vasavada AR, Paige DA (2014) Lunar cold spots: Granular flow features and extensive insulating materials surrounding young craters. Icarus 231:221–231

Baratoux D, Reimold WU (2016) The current state of knowledge about shatter cones: Introduction to the special issue. Meteorit Planet Sci 51:1389–1434

Barker MK, Mazarico E, Neumann GA, Zuber MT, Haruyama J, Smith DE (2016) A new lunar digital elevation model from the Lunar Orbiter Laser Altimeter and SELENE Terrain Camera. Icarus 273:346–355

Basu A, McKay DS (1985) Chemical variability and origin of agglutinitic glass. Proc Lunar Planet Sci Conf 16:87–94

Basu A, Wentworth SJ, McKay DS (2002) Heterogeneous agglutinitic glass and the fusion of the finest fraction (F3) model. Meteorit Planet Sci 37:1835–1842

Bierson CJ, Phillips RJ, Nimmo F, Besserer J, Milbury C, Keane JT, Soderblom JM, Zuber MT (2016) Interactions between complex craters and the lunar crust: Analysis using GRAIL data. J Geophys Res 121:1488–1497

Bray VJ, Tornabene LL, Keszthelyi LP, McEwen AS, Hawke BR, Giguere TA, Kattenhorn SA, Garry WB, Rizk B, Caudill CM, Gaddis LR (2010) New insight into lunar impact melt mobility from the LRO camera. Geophys Res Lett 37:L21202

Bray VJ, Atwood-Stone C, McEwen AM (2012) Investigating the transition from central peak to peak-ring basins using central feature volume measurements from the Global Lunar DTM 100 m. Geophys Res Lett 39:L21201

Bray VJ, Atwood-Stone C, Neish CD, Artemieva NA, McEwen AS, McElwaine JN (2018) Lobate impact melt flows within the extended ejecta blanket of Pierazzo crater. Icarus 301:26–36

Cahill JTS, Lucey PG, Wieczorek MA (2009) Compositional variations of the lunar crust: Results from radiative transfer modeling of central peak spectra. J Geophys Res 114: L21202

Calzada-Diaz A, Joy KH, Crawford IA, Nordheim TA (2015) Constraining the source regions of lunar meteorites using orbital geochemical data. Meteorit Planet Sci 228:214–228

Carter LM, Neish CD, Bussey DB, Spudis PD, Patterson GW, Cahill JT, Raney RK (2012) Initial observations of lunar impact melts and ejecta flows with the Mini-RF radar. J Geophys Res 117:E00H09

Chao ECT (1973) Geologic implications of the Apollo 14 Fra Mauro breccias and comparison with ejecta from the Ries Crater, Germany. J Res US Geol Surv 1:1–18

Chao ECT, Boreman JA, Desborough GA (1971) The petrology of unshocked and shocked Apollo 11 and Apollo 12 microbreccias. Proc Lunar Planet Sci Conf 2:797–816

Chappelow JE (2013) Simple impact crater shape determination from shadows. Meteorit Planet Sci 48:1863–1872

Cheek LC, Donaldson Hanna KL, Pieters CM, Head JW, Whitten JL (2013) The distribution and purity of anorthosite across the Orientale basin: New perspectives from Moon Mineralogy Mapper data. J Geophys Res 118:1805–1820

Cintala MJ, Grieve RAF (1998) Scaling impact melting and crater dimensions: Implications for the lunar cratering record. Meteorit Planet Sci 33:889–912

Cohen BA, van der Bogert CH, Bottke WF, Curran NM, Fassett CI, Hiesinger H, Joy KH, Mazrouei S, Nemchin A, Neumann GA, Norman MV, Zellner NEB (2023) Impact history of the Moon. Rev Mineral Geochem 89:373–400

Collins GS, Melosh HJ, Morgan J V, Warner MR (2002) Hydrocode simulations of Chicxulub Crater collapse and peak-ring formation. Icarus 157:24–33

Collins GS, Melosh HJ, Ivanov BA (2004) Modeling damage and deformation in impact simulations. Meteorit Planet Sci 39:217–231

Collins GS, Kenkmann T, Osinski GR, Wünnemann K (2008) Mid-sized complex crater formation in mixed crystalline-sedimentary targets: Insight from modeling and observation. Meteorit Planet Sci 43:1955–1977

Collins GS, Wünnemann K, Artemieva N, Pierazzo E (2012) Numerical modelling of impact processes. *In:* Osinski GR, Pierrazzo E (eds) Impact Cratering: Processes and Products. Blackwell Publishing Ltd, p 254–270

Delano JW (1986) Pristine lunar glasses: Criteria, data, and implications. Proc Lunar Planet Sci Conf 16:201–213

Delano JW, Zellner NE, Barra F, Olson E, Swindle TD, Tibbetts NJ, Whittet DC (2007) An integrated approach to understanding Apollo 16 impact glasses: Chemistry, isotopes, and shape. Meteorit Planet Sci 42:993–1004

Dence MR (1964) A comparative structural and petrographic study of probable Canadian meteorite craters. Meteoritics 2:249–270

Dence MR (1972) The nature and significance of terrestrial impact structures. Proc 24th Int Geol Congr Proc p 77–89

Denevi BW, Koeber SD, Robinson MS, Garry WB, Hawke BR, Tran TN, Lawrence SJ, Keszthelyi LP, Barnouin OS, Ernst CM, Tornabene LL (2012) Physical constraints on impact melt properties from Lunar Reconnaissance Orbiter Camera images. Icarus 219:665–675

Dhingra D (2015) Integrated mineralogy and high resolution geologic context of lunar impact melt deposits: Implications for crustal diversity and the impact cratering process. PhD Thesis, Brown University

Dhingra D, Pieters CM, Boardman JW, Head JW, Isaacson PJ, Taylor LA (2011) Compositional diversity at Theophilus Crater: Understanding the geological context of Mg-spinel bearing central peaks. Geophys Res Lett 38:L11201

Dhingra D, Pieters CM, Head JW, Isaacson PJ (2013) Large mineralogically distinct impact melt feature at Copernicus crater—Evidence for retention of compositional heterogeneity. Geophys Res Lett 40:1043–1048

Dhingra D, Head JW, Pieters CM (2017) Geological mapping of impact melt deposits at lunar complex craters Jackson and Tycho: Morphologic and topographic diversity and relation to the cratering process. Icarus 283:268–281

Donaldson Hanna KL, Pieters CM, Cheek LC, Bowles NE, Dhingra D (2014) Shocked anorthosite: Puzzling over its whereabouts. 45th Lunar Planet Sci Conf #2331

Dvorak J, Phillips RJ (1977) The nature of the gravity anomalies associated with large young lunar craters. Geophys Res Lett 4:380–382

Elbeshausen D, Wünnemann K, Collins GS (2009) Scaling of oblique impacts in frictional targets: Implications for crater size and formation mechanisms. Icarus 204:716–731

Fagan AL, Neal CR, Simonetti A, Donohue PH, O'Sullivan KM (2013) Distinguishing between Apollo 14 impact melt and pristine mare basalt samples by geochemical and textural analyses of olivine. Geochim Cosmochim Acta 106:429–445

Fassett CI, Thomson BJ (2014) Crater degradation on the lunar maria: Topographic diffusion and the rate of erosion on the Moon. J Geophys Res 119:2255–2271

Fernandes VA, Fritz J, Weiss BP, Garrick-Bethell I, Shuster DL (2013) The bombardment history of the Moon as recorded by ^{40}Ar–^{39}Ar chronology. Meteorit Planet Sci 48:241–269

Freed AM, Johnson BC, Blair DM, Melosh HJ, Neumann GA, Phillips RJ, Solomon SC, Wieczorek MA, Zuber MT (2014) The formation of lunar mascon basins from impact to contemporary form. J Geophys Res 119:L11201

French BM (1998) Traces of Catastrophe: A handbook of Shock-Metamorphic Effects in Terrestrial Meteorite Impact Structures, LPI Contribution No. 954. Lunar and Planetary Institute, Houston

French BM, Koeberl C (2010) The convincing identification of terrestrial meteorite impact structures: What works, what doesn't, and why. Earth Sci Rev 98:123–170

Fritz J, Greshake A, Fernandes VA (2017) Revising the shock classification of meteorites. Meteorit Planet Sci 52:1216–1232

Fritz J, Assis Fernandes V, Greshake A, Holzwarth A, Böttger U (2019) On the formation of diaplectic glass: Shock and thermal experiments with plagioclase of different chemical compositions. Meteorit Planet Sci 54:1533–1547

Gault DE, Quaide WL, Oberbeck VR (1968) Impact cratering mechanics and structures. *In:* French BM, Short NM (eds) Shock Metamorphism of Natural Materials. Mono Book Corp., Baltimore, p 87–99

Gault DE, Wedekind JA (1978) Experimental studies of oblique impacts. Proc Lunar Planet Sci Conf 9:3843–3875

Ghent RR, Gupta V, Campbell BA, Ferguson SA, Brown JC, Fergason RL, Carter LM (2010) Generation and emplacement of fine-grained ejecta in planetary impacts. Icarus 209:818–835

Ghent RR, Hayne PO, Bandfield JL, Campbell BA, Allen CC, Carter LM, Paige DA (2014) Constraints on the recent rate of lunar ejecta breakdown and implications for crater ages. Geology 42:1059–1062

Ghent RR, Carter LM, Bandfield JL, Udovicic CT, Campbell BA (2016) Lunar crater ejecta: Physical properties revealed by radar and thermal infrared observations. Icarus 273:182–195

Gilbert GK (1893) The Moon's face; a study of the origin of its features. Bull Philisophical Soc Washing 12:241–292

Gleißner P, Becker H (2017) Formation of Apollo 16 impactites and the composition of late accreted material: Constraints from Os isotopes, highly siderophile elements and sulfur abundances. Geochemica Cosmochim Acta 200:1–24

Gombosi DJ, Baldwin SL, Watson EB, Swindle TD, Delano JW, Roberge WG (2015) Argon diffusion in Apollo 16 impact glass spherules: Implications for $^{40}Ar/^{39}Ar$ dating of lunar impact events. Geochemica Cosmochim Acta 148:251–268

Gong S, Wieczorek MA, Nimmo F, Kiefer WS, Head JW, Huang C, Smith DE, Zuber MT (2016) Thicknesses of mare basalts on the Moon from gravity and topography. J Geophys Res Planets121:854-870

Green RO, Pieters C, Mouroulis P, Eastwood M, Boardman J, Glavich T, Isaacson P, Annadurai M, Besse S, Barr D, Buratti B (2011) The Moon Mineralogy Mapper (M3) imaging spectrometer for lunar science: Instrument description, calibration, on-orbit measurements, science data calibration and on-orbit validation. J Geophys Res 116:E10

Grieve RAF (1978) The melt rocks at Brent Crater, Ontario, Canada. Proc Lunar Planet Sci Conf 9:2579–2608

Grieve RAF, Cintala MJ (1981) A method for estimating the initial impact conditions of terrestrial cratering events, exemplified by its application to Brent crater, Ontario. Proc Lunar Planet Sci Conf 12:1607–1621

Grieve RAF, Cintala MJ (1992) An analysis of differential impact melt-crater scaling and implications for the terrestrial impact record. Meteoritics 27:526–538

Grieve RAF, Garvin JB (1984) A geometric model for excavation and modification at terrestrial simple impact craters. J Geophys Res 89:11561–11572

Grieve RAF, Osinski GR (2020) The Upper Contact Unit of the Sudbury Igneous Complex in the Garson region: Constraints on the depth of origin of a peak ring at the Sudbury impact structure. Meteorit Planet Sci 55:1734-1748

Grieve RAF, Therriault A (2004) Observations at terrestrial impact structures: Their utility in constraining crater formation. Meteorit Planet Sci 39:199–216

Grieve RAF, Therriault AM (2012) Impactites: Their characteristics and spatial distribution. *In:* Osinski GR, Pierazzo E (eds) Impact Cratering: Processes and Products. Wiley-Blackwell, Oxford, United Kingdom, p 90–105

Grieve RAF, Dence MR, Robertson PB (1977) Cratering processes: As interpreted from the occurrences of impact melts. *In:* Roddy DJ, Pepin RO, Merrill RB (eds) Impact and Explosion Cratering. Pergamon Press, New York, p 791–814

Grieve RAF, Stöffler D, Deutsch A (1991) The Sudbury structure: Controversial or misunderstood? J Geophys Res 96:22753–22764

Grieve RAF, Langenhorst F, Stöffler D (1996) Shock metamorphism of quartz in nature and experiment: II. Significance in geoscience. Meteorit Planet Sci 31:6–35

Güldemeister N, Wünnemann K, Durr N, Hiermaier S (2013) Propagation of impact-induced shock waves in porous sandstone using mesoscale modeling. Meteorit Planet Sci 48:115–133

Hartmann WK, Kuiper GP (1962) Concentric structures surrounding lunar basins. Commun Lunar Planet Lab 1:51–66

Hartmann WK, Quantin C, Mangold N (2007) Possible long-term decline in impact rates 2. Lunar impact-melt data regarding impact history. Icarus 186:11–23

Haruyama J, Matsunaga T, Ohtake M, Morota T, Honda C, Yokota Y, Torii M, Ogawa Y (2008) Global lunar-surface mapping experiment using the Lunar Imager/Spectrometer on SELENE. Earth, Planets Sp 60:243–255

Hasebe N, Shibamura E, Miyachi T, Takashima T, Kobayashi M, Okudaira O, Yamashita N, Kobayashi S, Ishizaki T, Sakurai K, Miyajima M (2008) Gamma-ray spectrometer (GRS) for lunar polar orbiter SELENE. Earth, Planets Sp 60:299–312

Hawke BR, Head JW (1977) Impact melt on lunar crater rims. *In:* Roddy DJ, Pepin RO, Merrill RB (eds) Impact and Explosion Cratering. Pergamon Press, New York, p 815–841

Hayne PO, Bandfield JL, Siegler MA, Vasavada AR, Ghent RR, Williams JP, Greenhagen BT, Aharonson O, Elder CM, Lucey PG, Paige DA (2017) Global Regolith Thermophysical Properties of the Moon From the Diviner Lunar Radiometer Experiment. J Geophys Res 122:2371–2400

Head JW (2010) Transition from complex craters to multi-ringed basins on terrestrial planetary bodies: Scale-dependent role of the expanding melt cavity and progressive interaction with the displaced zone. Geophys Res Lett 37:L02203

Henriksen MR, Manheim MR, Burns KN, Seymour P, Speyerer EJ, Deran A, Boyd AK, Howington-Kraus E, Rosiek MR, Archinal BA, Robinson MS (2017) Extracting accurate and precise topography from LROC narrow angle camera stereo observations. Icarus 283:122–137

Hiesinger HV, Van Der Bogert CH, Pasckert JH, Funcke L, Giacomini L, Ostrach LR, Robinson MS (2012) How old are young lunar craters? J Geophys Res 117:L02203

Hiesinger H, van der Bogert CH, Michael G, Schmedemann N, Iqbal W, Robbins SJ, Ivanov B, Williams J-P, Zanetti M, Plescia J, Ostrach LR, Head III JW (2023) The lunar cratering chronology. Rev Mineral Geochem 89:401–451

Holsapple KA (1993) The scaling of impact processes in planetary sciences. Annu Rev Earth Planet Sci 21:333–373

Hörz F, Cintala MJ (1997) Impact experiments related to the evolution of planetary regoliths. Meteorit Planet Sci 32:179–209

Hörz F, Ostertag R, Rainey DA (1983) Bunte breccia of the Ries: Continuous deposits of large impact craters. Rev Geophys Space Phys 21:1667–1725

Huang DA, Zellner NE, Hirabayashi M, Richardson JE, Fassett CI (2018) No change in recent lunar impact flux from modeling impact glass spherule ages. Geophys Res Lett 45:6805–6813

Hurwitz DM, Kring DA (2014) Differentiation of the South Pole–Aitken basin impact melt sheet: Implications for lunar exploration. J Geophys Res 119:1110–1133

Innes MJS (1961) The use of gravity methods to study the underground structure and impact energy of meteorite craters. J Geophys Res 66:2225–2239

Jaret SJ, Woerner WR, Phillips BL, Ehm L, Nekvasil H, Wright SP, Glotch TD (2015) Maskelynite formation via solid-state transformation: Evidence of infrared and X-ray anisotropy. J Geophys Res 120: 570–587

Jaret SJ, Johnson JR, Sims M, DiFrancesco N, Glotch TD (2018) Microspectroscopic and petrographic comparison of experimentally shocked albite, andesine, and bytownite. J Geophys Res 123:1701–1722

Johnson BC, Melosh HJ (2012) Formation of spherules in impact produced vapor plumes. Icarus 217:416–430

Johnson BC, Melosh HJ (2014) Formation of melt droplets, melt fragments, and accretionary impact lapilli during a hypervelocity impact. Icarus 228:347–363

Johnson BC, Blair DM, Collins GS, Melosh HJ, Freed AM, Taylor GJ, Head JW, Wieczorek MA, Andrews-Hanna JC, Nimmo F, Keane JT (2016) Formation of the Orientale lunar multiring basin. Science 354:441–444

Johnson BC, Andrews-Hanna JC, Collins GS, Freed AM, Melosh HJ, Zuber MT (2018) Controls on the formation of lunar multiring basins. J Geophys Res 123:3035–3050

Johnson JR, Jaret SJ, Glotch TD, Sims M (2020) Raman and infrared microspectroscopy of experimentally shocked basalts. J Geophys Res 125:e2019JE006240

Jourdan F, Renne PR, Reimold WU (2009) An appraisal of the ages of terrestrial impact structures. Earth Planet Sci Lett 286:1–13

Joy KH, Crawford IA, Russell SS, Kearsley AT (2010) Lunar meteorite regolith breccias : An in situ study of impact melt composition using LA-ICP-MS with implications for the composition of the lunar crust. Meteorit Planet Sci 45:917–946

Joy KH, Gross J, Korotev RL, Zeigler RA, McCubbin FM, Snape JF, Curran NM, Pernet-Fisher JF, Arai T (2023) Lunar meteorites. Rev Mineral Geochem 89:509–562

Kalynn J, Johnson CL, Osinski GR, Barnouin O (2013) Topographic characterization of lunar complex craters. Geophys Res Lett 40:38–42

Kayama M, Nishido H, Sekine T, Nakazato T, Gucsik A, Ninagawa K (2012) Shock barometer using cathodoluminescence of alkali feldspar. J Geophys Res 117:E09004

Keller LP, McKay DS (1992) Micrometer-sized glass spheres in Apollo 16 soil 61181: Implications for impact volatilization and condensation. Proc Lunar Planet Sci Conf 22:137–141

Kenkmann T, Collins GS, Wünnemann K (2012) The modification stage of crater formation. *In:* Osinski GR, Pierazzo E (eds) Impact Cratering: Processes and Products. Wiley-Blackwell, Chichester, p 60–75

Kenkmann T, Poelchau M, Wulf G (2014) Structural geology of impact craters. J Struct Geol 62:156–182

Kenkmann T, Deutsch A, Thoma K, Ebert M, Poelchau MH, Buhl E, Carl ER, Danilewsky AN, Dresen G, Dufresne A, Durr N (2018) Experimental impact cratering: A summary of the major results of the MEMIN research unit. Meteorit Planet Sci 53:1543–1568

Kieffer SW (1971) Shock metamorphism of the Coconino sandstone at Meteor Crater, Arizona. J Geophys Res 76:5449–5473

Korotev RL, Zeigler RA, Floss C (2010) On the origin of impact glass in the Apollo 16 regolith. Geochim Cosmochim Acta 74:7362–7388

Kring DA, Kramer GY, Collins GS, Potter RW, Chandnani M (2016) Peak-ring structure and kinematics from a multi-disciplinary study of the Schrödinger impact basin. Nat Commun 7:13161

Krüger T, Kenkmann T, Hergarten S (2017) Structural uplift and ejecta thickness of lunar mare craters: New insights into the formation of complex crater rims. Meteorit Planet Sci 52:2220–2240

Krüger T, Hergarten S, Kenkmann T (2018) Deriving morphometric parameters and the simple-to-complex transition diameter from a high resolution, global database of fresh lunar impact craters ≥ ~ 3 km. J Geophys Res 123:2667–2690

Lai J, Xu Y, Zhang X, Xiao L, Yan Q, Meng X, Zhou B, Dong Z, Zhao D (2019) Comparison of dielectric properties and structure of lunar regolith at Chang'e-3 and Chang'e-4 landing sites revealed by Ground-Penetrating Radar. Geophys Res Lett 46:12783–12793

Langenhorst F (2002) Shock metamorphism of some minerals: Basic introduction and microstructural observations. Bull Czech Geol Surv 77:265–282

Lin H, Lin Y, Yang W, He Z, Hu S, Wei Y, Xu R, Zhang J, Liu X, Yang J, Xing Y (2020) New insight into lunar regolith-forming processes by the Lunar Rover Yutu-2. Geophys Res Lett 47:e2020GL087949

Losiak A, Wilhelms DE, Byrn CJ, Thaisen K, Weider SZ, Kohout T, O'Sullivan K, Kring DA (2009) A new lunar crater database. Abstract #1532. Paper presented at the 40th Lunar and Planetary Science Conference, Houston, TX. Mader MM, Osinski GR (2018) Impactites of the Mistastin Lake impact structure: Insights into impact ejecta emplacement. Meteorit Planet Sci 53:2492–2518

Mahanti P, Robinson MS, Stelling R (2015) How old are small lunar craters? A depth-to-diameter ratio based analysis. 46th Lunar Planet Sci Conf #1615
Mahanti P, Lanjewar K, Thompson T (2018) Classification of small lunar crater morphological state by deep learning. *In:* Planetary Science Informatics and Data Analytics Conference #6028
Maloof AC, Stewart ST, Weiss BP, Soule SA, Swanson-Hysell NL, Louzada KL, Garrick-Bethell I, Poussart PM (2010) Geology of Lonar Crater, India. Geol Soc Am Bull 122:109–126
Martin DJ, Pernet-Fisher JF, Joy KH, Wogelius RA, Morlok A, Hiesinger H (2017) Investigating the shock histories of lunar meteorites Miller Range 090034, 090070, and 090075 using petrography, geochemistry, and micro-FTIR spectroscopy. Meteorit Planet Sci 52:1103–1124
Mazrouei S, Ghent RR, Bottke WF, Parker AH, Gernon TM (2019) Earth and Moon impact flux increased at the end of the Paleozoic. Science 363:253–257
Melosh HJ (1989) Impact Cratering: A Geologic Process. Oxford University Press, New York
Melosh HJ (1985) Impact cratering mechanics: Relationship between the shock wave and excavation flow. Icarus 62:339–343
Melosh HJ (2012) The contact and compression stage of impact cratering. *In:* Osinski GR, Pierazzo E (eds) Impact Cratering: Processes and Products. Wiley-Blackwell, p 32–42
Melosh HJ, Ivanov BA (1999) Impact crater collapse. Annu Rev Earth Planet Sci 27:385–415
Melosh HJ, McKinnon W (1978) The mechanics of ringed basin formation. Geophys Res Lett 5:985–988
Melosh HJ, Freed AM, Johnson BC, Blair DM, Andrews-Hanna JC, Neumann GA, Phillips RJ, Smith DE, Solomon SC, Wieczorek MA, Zuber MT (2013) The origin of lunar mascon basins. Science 340:1552–1555
Michael G, Basilevsky A, Neukum G (2018) On the history of the early meteoritic bombardment of the Moon: Was there a terminal lunar cataclysm? Icarus 302:80–103
Milbury C, Johnson BC, Melosh HJ, Collins GS, Blair DM, Soderblom JM, Nimmo F, Bierson CJ, Phillips RJ, Zuber MT (2015) Preimpact porosity controls the gravity signature of lunar craters. Geophys Res Lett 42:9711–9716
Morgan JV, Gulick SP, Bralower T, Chenot E, Christeson G, Claeys P, Cockell C, Collins GS, Coolen MJ, Ferrière L, Gebhardt C (2016) The formation of peak rings in large impact craters. Science 354:878–882
Morse ZR, Osinski GR, Tornabene LL (2018) New morphological mapping and interpretation of ejecta deposits from Orientale Basin on the Moon. Icarus 299:253–271
Muller PM, Sjogren WL (1968) Mascons: Lunar Mass Concentrations. Science 161:680–684
Neal CR, Donohue P, Fagan AL, O'Sullivan K, Oshrin J, Roberts S (2015) Distinguishing between basalts produced by endogenic volcanism and impact processes: A non-destructive method using quantitative petrography of lunar basaltic samples. Geochim Cosmochim Acta 148:62–80
Neish CD, Madden J, Carter LM, Hawke BR, Giguere T, Bray VJ, Osinski GR, Cahill JT (2014) Global distribution of lunar impact melt flows. Icarus 239:105–117
Neish CD, Hamilton CW, Hughes SS, Nawotniak SK, Garry WB, Skok JR, Elphic RC, Schaefer E, Carter LM, Bandfield JL, Osinski GR (2017) Terrestrial analogues for lunar impact melt flows. Icarus 281:73–89
Neumann GA, Zuber MT, Wieczorek MA, Head JW, Baker DM, Solomon SC, Smith DE, Lemoine FG, Mazarico E, Sabaka TJ, Goossens S (2015) Lunar impact basins revealed by Gravity Recovery and Interior Laboratory measurements. Sci Adv 1: e1500852
Norman MD (1982) Petrology of suevitic lunar breccia 67016. Proc Lunar Planet Sci Conf 12:235–252
Norman MD, Taylor LA, Shih CY, Nyquist LE (2016) Crystal accumulation in a 4.2Ga lunar impact melt. Geochemica Cosmochim Acta 172:410–429
Nozette S, Spudis P, Bussey B, Jensen R, Raney K, Winters H, Lichtenberg CL, Marinelli W, Crusan J, Gates M, Robinson M (2010) The Lunar Reconnaissance Orbiter Miniature Radio Frequency (Mini-RF) Technology Demonstration. Space Sci Rev 150:285–302
Oberbeck VR (1975) The role of ballistic erosion and sedimentation in lunar stratigraphy. Rev Geophys Sp Phys 13:337–362
Öhman T (2015) LPI crater database. Houston, TX: Lunar & Planetary Institute
Ohtake M, Haruyama J, Matsunaga T, Yokota Y, Morota T, Honda C (2008) Performance and scientific objectives of the SELENE (KAGUYA) Multiband Imager. Earth, Planets Sp 60:257–264
Ohtake M, Matsunaga T, Haruyama J, Yokota Y, Morota T, Honda C, Ogawa Y, Torii M, Miyamoto H, Arai T, Hirata N (2009) The global distribution of pure anorthosite on the Moon. Nature 461:236–240
Osinski GR (2004) Impact melt rocks from the Ries impact structure, Germany: An origin as impact melt flows? Earth Planet Sci Lett 226:529–543
Osinski GR, Grieve RAF (2019) Impact Earth: A new resource for outreach, teaching, and research. Elements 15:70–71
Osinski GR, Ferrière L (2016) Shatter cones: (Mis)understood? Sci Adv 2:e1600616
Osinski GR, Pierazzo E (2012) Impact Cratering: Processes and Products. Wiley-Blackwell
Osinski GR, Spray JG (2005) Tectonics of complex crater formation as revealed by the Haughton impact structure, Devon Island, Canadian High Arctic. Meteorit Planet Sci 40:1813–1834
Osinski GR, Grieve RAF, Spray JG (2004) The nature of the groundmass of surficial suevites from the Ries impact structure, Germany, and constraints on its origin. Meteorit Planet Sci 39:1655–1684
Osinski GR, Spray JG, Lee P (2005) Impactites of the Haughton impact structure, Devon Island, Canadian High Arctic. Meteorit Planet Sci 40:1789–1812

Osinski GR, Grieve RA, Collins GS, Marion C, Sylvester P (2008) The effect of target lithology on the products of impact melting. Meteorit Planet Sci 43:1939–1954
Osinski GR, Tornabene LL, Grieve RAF (2011) Impact ejecta emplacement on the terrestrial planets. Earth Planet Sci Lett 310:167–181
Osinski GR, Grieve RAF, Tornabene LL (2012) Excavation and impact ejecta emplacement. *In:* Osinski GR, Pierazzo E (eds) Impact Cratering: Processes and Products. Wiley-Blackwell, Chichester, p 43–59
Osinski GR, Grieve RAF, Chanou A, Sapers HM (2016) 1. The "suevite" conundrum, Part 1: The Ries suevite and Sudbury Onaping Formation compared. Meteorit Planet Sci 51:2316–2333
Osinski GR, Grieve RA, Bleacher JE, Neish CD, Pilles EA, Tornabene LL (2018) Igneous rocks formed by hypervelocity impact. J Volcanol Geotherm Res 353:25–54
Osinski GR, Silber EA, Clayton J, Grieve RA, Hansen K, Johnson CL, Kalynn J, Tornabene LL (2019) Transitional impact craters on the Moon: Insight into the effect of target lithology on the impact cratering process. Meteorit Planet Sci 54:573–591
Osinski GR, Grieve RA, Hill PJ, Simpson SL, Cockell C, Christeson GL, Ebert M, Gulick S, Melosh HJ, Riller U, Tikoo SM (2020) Explosive interaction of impact melt and seawater following the Chicxulub impact event. Geology 48:108–112
Paige DA, Foote MC, Greenhagen BT, Schofield JT, Calcutt S, Vasavada AR, Preston DJ, Taylor FW, Allen CC, Snook KJ, Jakosky BM (2010) The Lunar Reconnaissance Orbiter Diviner Lunar Radiometer Experiment. Space Sci Rev 150:125–160
Pernet-Fisher JF, Joy KH, Martin DJ, Donaldson Hanna KL (2017) Assessing the shock state of the lunar highlands: Implications for the petrogenesis and chronology of crustal anorthosites. Nat Sci Reports 7:5888
Pickersgill AE, Flemming RL, Osinski GR (2015a) Toward quantification of strain-related mosaicity in shocked lunar and terrestrial plagioclase by in situ micro-X-ray diffraction. Meteorit Planet Sci 50:1851–1862
Pickersgill AE, Osinski GR, Flemming RL (2015b) Shock effects in plagioclase feldspar from the Mistastin Lake impact structure, Canada. Meteorit Planet Sci 50:1546–1561
Pierazzo E, Melosh HJ (2000a) Hydrocode modeling of oblique impacts: The fate of the projectile. Meteorit Planet Sci 35:117–130
Pierazzo E, Melosh HJ (2000b) Melt production in oblique impacts. Icarus 145:252–261
Pierazzo E, Vickery AM, Melosh HJ (1997) A reevaluation of impact melt production. Icarus 127:408–423
Pierazzo E, Artemieva N, Asphaug E, Baldwin EC, Cazamias J, Coker R, Collins GS, Crawford DA, Davison T, Elbeshausen D, Holsapple KA (2008) Validation of numerical codes for impact and explosion cratering: Impacts on strengthless and metal targets. Meteorit Planet Sci 43:1917–1938
Pike R (1977) Size-dependence in the shape of fresh impact craters on the Moon. *In:* Merrill RB, Pepin RDJ, Pepin RO (eds) Impact and Explosion Cratering. pergamon press, New York, p 489–509
Pike RJ (1976) Crater dimensions from Apollo data and supplemental sources. Moon 15:463–477
Pike RJ (1980a) Formation of complex impact craters: Evidence from Mars and other planets. Icarus 43:1–19
Pike RJ (1980b) Control of crater morphology by gravity and target type—Mars, Earth, Moon. Proc Lunar Planet Sci Conf 11:2159–2189
Pike RJ, Spudis PD (1987) Basin-ring spacing on the Moon, Mercury, and Mars. Earth Moon Planets 39:129–194
Pilkington M, Grieve RAF (1992) The geophysical signature of terrestrial impact craters. Rev Geophys 30:161–181
Pittarello L, Daly L, PickersgilL AE, Ferrière L, Lee MR (2020) Shock metamorphism in plagioclase and selective amorphization. Meteorit Planet Sci 55:1103–1115
Plescia JB, Cintala MJ (2012) Impact melt in small lunar highland craters. J Geophys Res 117:E00H12
Plescia JB, Robinson MS (2011) New constraints on the absolute lunar cratering chronology. 42nd Lunar Planet Sci Conf #1839
Plescia JB, Cahill J, Greenhagen B, Hayne P, Mahanti P, Robinson MS, Spudis PD, Siegler M, Stickle A, Williams JP, Zanetti M, Zellner N (2023) Lunar surface processes. Rev Mineral Geochem 89:651–690
Poelchau MH, Kenkmann T, Hoerth T, Schäfer F, Rudolf M, Thoma K (2014) Impact cratering experiments into quartzite, sandstone and tuff: The effects of projectile size and target properties on spallation. Icarus 242:211–224
Potter RW, Kring DA, Collins GS, Kiefer WS, McGovern PJ (2013) Numerical modeling of the formation and structure of the Orientale impact basin. J Geophys Res 118:963–979
Puchtel IS, Walker RJ, James OB, Kring DA (2008) Osmium isotope and highly siderophile element systematics of lunar impact melt breccias: Implications for the late accretion history of the Moon and Earth. Geochemica Cosmochim Acta 72:3022–3042
Quaide WL, Gault DE, Schmidt RA (1965) Gravitative effects on lunar impact structures. Ann New York Acad Sci 123:563–572
Riller U, Poelchau MH, Rae AS, Schulte FM, Collins GS, Melosh HJ, Grieve RA, Morgan JV, Gulick SP, Lofi J, Diaw A (2018) Rock fluidization during peak-ring formation of large impact structures. Nature 562:511–518
Robinson MS, Brylow SM, Tschimmel M, Humm D, Lawrence SJ, Thomas PC, Denevi BW, Bowman-Cisneros E, Zerr J, Ravine MA, Caplinger MA (2010) Lunar Reconnaissance Orbiter Camera (LROC) Instrument Overview. Space Sci Rev 150:81–124
Robinson KL, Treiman AH, Joy KH (2012) Basaltic fragments in lunar feldspathic meteorites: Connecting sample analyses to orbital remote sensing. Meteorit Planet Sci 47:387–399

Robinson MS, Thomas PC, Plescia JB, Denevi BW, Burns KN, Bowman-Cisneros E, Henriksen MR, Van der Bogert CH, Hiesinger H, Mahanti P, Stelling RW (2016) An exceptional grouping of lunar highland smooth plains: Geography, morphology, and possible origins. Icarus 273:121–134
Roddy DJ, Pepin RO, Merrill RB (1977) Impact and Explosion Cratering. Pergamom Press, New York
Rubin AE (1997) Mineralogy of meteorite groups. Meteorit Planet Sci 32:231–247
Rubin AE (2015) Maskelynite in asteroidal, lunar and planetary basaltic meteorites: An indicator of shock pressure during impact ejection from their parent bodies. Icarus 257:221–229
Ryder G, Delano JW, Warren PH, Kallemeyn GW, Dalrymple GB (1996) A glass spherule of questionable impact origin from the Apollo 15 landing site: Unique target mare basalt. Geochemica Cosmochim Acta 60:673–710
Sapers HM, Osinski GR, Banerjee NR, Ferrière L, Lambert P, Izawa MR (2014) Revisiting the Rochechouart impact structure, France. Meteorit Planet Sci 49:2152–2168
Sato H, Robinson MS, Hapke B, Denevi BW, Boyd AK (2014) Resolved Hapke parameter maps of the Moon. J Geophys Res 119:1775–1805
Scholten F, Oberst J, Matz KD, Roatsch T, Wählisch M, Speyerer EJ, Robinson MS (2012) GLD100: The near-global lunar 100 m raster DTM from LROC WAC stereo image data. J Geophys Res 117:E12
Schultz PH, Gault DE (1975) Seismic effects from major basin formations on the Moon and Mercury. Moon 12:159–177
Schultz PH, Mendell WW (1978) Orbital infrared observations of lunar craters and possible implications for impact ejecta emplacement. Proc Lunar Planet Sci Conf 9:2857–2883
See TH, Hörz F (1988) Formation of agglutinate-like particles in an experimental regolith. Proc Lunar Planet Sci Conf 18:423–434
Senft LE, Stewart ST (2009) Dynamic fault weakening and the formation of large impact craters. Earth Planet Sci Lett 287:471–482
Sharpton VL (2014) Outcrops on lunar crater rims: Implications for rim construction mechanisms, ejecta volumes and excavation depths. J Geophys Res 119:154–168
Shoemaker EM (1960) Penetration mechanics of high velocity meteorites, illustrated by Meteor Crater, Arizona. *In:* International Geological Congress, Copenhagen, p 418–434
Shoemaker EM (1963) Impact mechanics at Meteor Crater, Arizona. *In:* Middlehurst BM, Kuiper GP (eds) The Moon, Meteorites and Comets. University of Chicago Press, Illinois, p 301–336
Shoemaker EM, Batson RM, Holt HE, Morris EC, Rennilson JJ, Whitaker EA (1969) Observations of the lunar regolith and the Earth from the television camera on Surveyor 7. J Geophys Res 74:6081–6119
Siegert S, Branney MJ, Hecht L (2017) Density current origin of a melt-bearing impact ejecta blanket (Ries suevite, Germany). Geology 45:855–858
Silber EA, Osinski GR, Johnson BC, Grieve RAF (2017) Effect of impact velocity and acoustic fluidization on the simple-to-complex transition of lunar craters. J Geophys Res 122:800–821
Silber EA, Zanetti M, Osinski GR, Johnson BC, Grieve RA (2018) A combined modeling and observational study of the effect of impact velocity on production of melt in simple-to-complex lunar craters. 49th Lunar Planet Sci Conf #1401
Smith DE, Zuber MT, Neumann GA, Lemoine FG, Mazarico E, Torrence MH, McGarry JF, Rowlands DD, Head JW, Duxbury TH, Aharonson O (2010) Initial observations from the Lunar Orbiter Laser Altimeter (LOLA). Geophys Res Lett 37:L18204
Soderblom JM, Evans AJ, Johnson BC, Melosh HJ, Miljković K, Phillips RJ, Andrews-Hanna JC, Bierson CJ, Head JW, Milbury C, Neumann GA (2015) The fractured Moon: Production and saturation of porosity in the lunar highlands from impact cratering. Geophys Res Lett 42:6939–6944
Solomon SC, Head JW (1979) Vertical movement in mare basins: Relation to mare emplacement, basin tectonics, and lunar thermal history. J Geophys Res 84:1667–1682
Spudis PD (1993) The Geology of Multi-Ring Impact Basins. Cambridge University Press, Cambridge
Spudis PD, Martin DJP, Kramer G (2014) Geology and composition of the Orientale Basin impact melt sheet. J Geophys Res 119:19–29
Stöffler D (1972) Deformation and transformation of rock-forming minerals by natural and experimental shock processes: I. Behavior of minerals under shock compression. Fortschritte der Mineral 49:50–113
Stöffler D (1984) Glasses formed by hypervelocity impact. J Non Cryst Solids 67:465–502
Stöffler D, Grieve RAF (2007) Impactites. *In:* Fettes D, Desmons J (eds) Metamorphic Rocks. Cambridge University Press, Cambridge, p 82–92
Stöffler D, Langenhorst F (1994) Shock metamorphism of quartz in nature and experiment: 1. Basic observation and theory. Meteoritics 29:155–181
Stöffler D, Knöll HD, Maerz U (1979) Terrestrial and lunar impact breccias and the classification of lunar highland rocks. Proc Lunar Planet Sci Conf 10:639–675
Stöffler D, Knöll HD, Marvin UB, Simonds CH, Warren PH (1980) Recommended classification and nomenclature of lunar highland rocks—A committee report. Proceedings, Conf Lunar Highlands Crust 51–70
Stöffler D, Ryder G, Ivanov BA, Artemieva NA, Cintala MJ, Grieve RA (2006) Cratering history and lunar chronology. Rev Mineral Geochem 60:519–596

Stopar JD, Hawke BR, Robinson MS, Denevi BW, Giguere TA, Koeber SD (2014) Occurrence and mechanisms of impact melt emplacement at small lunar craters. Icarus 243:337–357
Stopar JD, Robinson MS, Barnouin OS, McEwen AS, Speyerer EJ, Henriksen MR, Sutton SS (2017) Relative depths of simple craters and the nature of the lunar regolith. Icarus 298:34–48
Therriault AM, Fowler AD, Grieve RAF (2002) The Sudbury Igneous Complex: A differentiated impact melt sheet. Econ Geol 97:1521–1540
Timms NE, Erickson TM, Zanetti MR, Pearce MA, Cayron C, Cavosie AJ, Reddy SM, Wittmann A, Carpenter PK (2017) Cubic zirconia in > 2370 °C impact melt records Earth's hottest crust. Earth Planet Sci Lett 477:52–58
Tompkins S, Pieters CM (1999) Mineralogy of the lunar crust: Results from Clementine. Meteorit Planet Sci 34:25–41
Trowbridge AJ, Johnson BC, Freed AM, Melosh HJ (2020) Why the lunar South Pole-Aitken Basin is not a mascon. Icarus 352:113995
Ulrich DR (1974) Study of recrystallization and devitrification of lunar glass. NASA Contractor Report, NASA-CR-134307
Van der Bogert CH, Hiesinger H, McEwen AS, Dundas C, Bray V, Robinson MS, Plescia JB, Reiss D, Klemm K, Team L (2017) Origin of discrepancies between crater size–frequency distributions of coeval lunar geologic units via target property contrasts. Icarus 298:49–63
Vaughan WM, Head JW (2014) Impact melt differentiation in the South Pole-Aitken basin*:* Some observations and speculations. Planet Space Sci 91:101–106
Vaughan WM, Head JW, Wilson L, Hess PC (2013) Geology and petrology of enormous volumes of impact melt on the Moon: A case study of the Orientale basin impact melt sea. Icarus 223:749–765
Venkatadri TK, James PB (2020) Variations of porosity in intermediate-sized lunar impact basins. Icarus 352:113953
Wahl D, Wieczorek MA, Wünnemann K, Oberst J (2020) Crustal porosity of lunar impact basins. J Geophys Res Planets 125:e2019JE006335
Walton EL, Herd CDK (2007) Dynamic crystallization of shock melts in Allan Hills 77005: Implications for melt pocket formation in Martian meteorites. Geochim Cosmochim Acta 71:5267–5285
Warren PH (1993) A concise compilation of petrologic information on possibly pristine nonmare Moon rocks. Am Mineral 78:360–376
White LF, Černok A, Darling JR, Whitehouse MJ, Joy KH, Cayron C, Dunlop J, Tait KT, Anand M (2020) Evidence of extensive lunar crust formation in impact melt sheets 4,330 Myr ago. Nat Astron 4:974–978
Wieczorek MA, Neumann GA, Nimmo F, Kiefer WS, Taylor GJ, Melosh HJ, Phillips RJ, Solomon SC, Andrews-Hanna JC, Asmar SW, Konopliv AS (2013) The crust of the Moon as seen by GRAIL. Science 339:671–675
Wiggins SE, Johnson BC, Bowling TJ, Melosh HJ, Silber EA (2019) Impact fragmentation and the development of the deep lunar megaregolith. J Geophys Res 124:941–957
Williams JP, Bandfield JL, Paige DA, Powell TM, Greenhagen BT, Taylor S, Hayne PO, Speyerer EJ, Ghent RR, Costello ES (2018) Lunar Cold Spots and Crater Production on the Moon. J Geophys Res 123:2380–2392
Wilson M (1993) Magmatic differentiation. J Geol Soc London 150:611–624
Wünnemann K, Collins GS, Melosh HJ (2006) A strain-based porosity model for use in hydrocode simulations of impacts and implications for transient crater growth in porous targets. Icarus 180:514–527
Wünnemann K, Collins GS, Osinski GR (2008) Numerical modelling of impact melt production on porous rocks. Earth Planet Sci Lett 269:529–538
Xie T, Shieh SR, Osinski GR (2017) Raman study of shock effects in lunar anorthite from the Apollo missions. 48th Lunar Planet Sci Conf #1596
Xie T, Osinski GR, Shieh SR (2020) Raman study of shock features in plagioclase feldspar from the Mistastin Lake impact structure, Canada. Meteorit Planet Sci 55:1471–1490
Zanetti M, Stadermann A, Jolliff B, Hiesinger H, Van der Bogert CH, Plescia J (2017) Evidence for self-secondary cratering of Copernican-age continuous ejecta deposits on the Moon. Icarus 298:64–77
Zellner NEB, Delano JW (2015) $^{40}Ar/^{39}Ar$ ages of lunar impact glasses: Relationships among Ar diffusivity, chemical composition, shape, and size. Geochem Cosmochim Acta 161:203–218
Zellner NEB, Spudis PD, Delano JW, Whittit DCB (2002) Impact glasses from the Apollo 14 landing site and implications for regional geology. J Geophys Res 107:5102–5115
Zhu M-H, Wünnemann K, Potter RWK (2015) Numerical modeling of the ejecta distribution and formation of the Orientale basin on the Moon. J Geophys Res 120:2118–2134
Zuber MT, Smith DE, Watkins MM, Asmar SW, Konopliv AS, Lemoine FG, Melosh HJ, Neumann GA, Phillips RJ, Solomon SC, Wieczorek MA (2013) Gravity field of the Moon from the Gravity Recovery and Interior Laboratory (GRAIL) Mission. Science 339:668–671